Progress in Nuclear Magnetic Resonance Spectroscopy 90-91 (2015) 32–48

Contents lists available at ScienceDirect

Progress in Nuclear Magnetic Resonance Spectroscopy

journal homepage: www.elsevier.com/locate/pnmrs

Magnetic resonance elastography (MRE) in cancer: Technique, analysis, and applications

Kay M. Pepin [a,*], Richard L. Ehman [b,1], Kiaran P. McGee [b,1]

[a] Mayo Graduate School, United States
[b] Department of Radiology, United States

Edited by David Gadian and Geoffrey Bodenhausen

ARTICLE INFO

Article history:
Received 9 March 2015
Accepted 16 June 2015
Available online 23 June 2015

Keywords:
Magnetic resonance elastography (MRE)
Oncology
Clinical applications
Tissue stiffness
Elasticity imaging

ABSTRACT

Tissue mechanical properties are significantly altered with the development of cancer. Magnetic resonance elastography (MRE) is a noninvasive technique capable of quantifying tissue mechanical properties in vivo. This review describes the basic principles of MRE and introduces some of the many promising MRE methods that have been developed for the detection and characterization of cancer, evaluation of response to therapy, and investigation of the underlying mechanical mechanisms associated with malignancy.

© 2015 Elsevier B.V. All rights reserved.

Contents

* Corresponding author. Tel.: +1 507 284 1146; fax: +1 507 284 9778.
E-mail addresses: pepin.kay@mayo.edu (K.M. Pepin), ehman.richard@mayo.edu (R.L. Ehman), mcgee.kiaran@mayo.edu (K.P. McGee).
[1] Tel.: +1 507 284 9770; fax: +1 507 284 9778.

http://dx.doi.org/10.1016/j.pnmrs.2015.06.001
0079-6565/© 2015 Elsevier B.V. All rights reserved.

1. Backgound

1.1. Introduction

It has been understood for several millennia that many physiological and pathological processes cause marked changes in the mechanical properties of tissue [1]. Physicians utilize touch to detect and diagnose abnormalities, notably cancer. Palpation contributes significantly to cancer detection as evidenced by the promotion and wide use of self-breast exams to monitor for the presence of disease [2]. While palpation is an incredibly powerful diagnostic tool, it is qualitative and limited by the sensitivity and experience of the practitioner. Additionally, unless it is combined with surgery, palpation can only be used to assess superficial pathologies.

In the past two decades a new, noninvasive imaging technique known as magnetic resonance elastography (MRE) has been developed to spatially resolve the mechanical properties of soft tissues [3]. MRE is particularly well suited for the study of cancer; the mechanical properties of tumors have implications for detection, characterization, prediction of response to treatment, and monitoring of therapy response. This review describes the basic principles of MRE, including the underlying physiological basis, data acquisition and analysis, limitations, and current clinical applications in cancer.

1.2. Clinical significance

Imaging plays a central role in oncology. Imaging is used not only for cancer screening, but also for diagnosis and staging, guiding cancer treatments, determining response to therapy, and monitoring for cancer recurrence. MR imaging techniques are broadly recognized as powerful and versatile tools for the noninvasive assessment of cancer morphology and functionality. However, even with the most advanced imaging techniques, significant needs remain, especially in the realm of oncology.

MR techniques are highly sensitive for the detection of cancer, but typically have low specificity for determination of tumor grade and malignant vs. benign status. Current clinical techniques employed in oncology use many different types of MR contrast. Dynamic contrast-enhanced MR (DCE-MRI) utilizes exogenous contrast agents (low molecular weight gadolinium chelates) administered in the blood stream that shortens the T_1 relaxation of blood, making it appear brighter on T_1-weighted MR images. The clinical application of DCE-MRI is to assess tumor angiogenesis, vascular permeability, and blood flow, based on the fact that tumor vessels are generally more permeable, heterogeneous in size, and tortuous than normal vessels. Diffusion-weighted imaging (DWI) employs the diffusivity of water as a quantitative parameter which reflects the diffusion of water molecules in tissue. A hallmark of cancer is increased cellularity and vascularity, both of which restrict diffusion resulting in lower apparent diffusion coefficient (ADC) values. Recent studies suggest that DWI may be sensitive to extracellular fibrosis, shape and size of the intercellular space, and other microscopic organization of tumor [4]. DWI has been used for tumor detection and characterization and for predicting and monitoring response to therapy. MR spectroscopic imaging (MRSI) is a technique that images tumor metabolic markers for cancer diagnosis, metabolic phenotyping, and characterization of the tumor microenvironment. The major limitation of MRSI is low spatial and temporal resolution due to low tissue concentrations of metabolites in tissue. An emerging tool in oncologic imaging is multiparametric MRI (MPMRI); the combination of conventional anatomical MRI and functional techniques. MPMRI improves the accuracy for identification, staging, and treatment planning in prostate cancer [5].

There is a clinical need for noninvasive imaging techniques for the accurate diagnosis and monitoring of cancer. The director of the National Cancer Institute and Nobel laureate Harold Varmus, M.D. has stated that "There is a tremendous need to incentivize development of validated and accepted diagnostics in order to keep pace with the explosion of new, targeted cancer drugs that are in the pipeline" [6]. MRE as a technique can provide contrast between the mechanical properties of normal and diseased tissue has the potential of playing an important role in the study and treatment of cancer.

2. Fundamentals of magnetic resonance elastography

Since the first publication in 1995 by Muthupillai et al. [3] which described a novel technique of imaging the propagation of mechanical waves in a gel phantom, MRE has been used to noninvasively quantify the mechanical properties of liver, brain, breast, heart, lung, spleen, kidneys, pancreas, uterus, muscle, and thyroid [7–19]. Clinically, MRE is routinely used for the noninvasive assessment of liver fibrosis and has replaced biopsy as the standard of care at the Mayo Clinic since 2007 [20]. The term 'elastography' was first introduced in 1991 to describe an ultrasound-based technique to determine a qualitative description of tissue strain resulting from external compression [21]. Elastography exists across several modalities including MR, ultrasound, optical imaging, and mechanical testing; however, an extensive description of each technique is outside the scope of this review.

2.1. Theoretical and biophysical basis of MRE

The field of mechanobiology is rapidly growing, incorporating mechanical properties with the study of the biology and function within normal physiology and disease. Tissue mechanics has been implicated in morphology, function, and the development of disease through mechanotransduction [22,23]. Noninvasive quantification of the mechanical properties of tissue may be useful in understanding the mechanisms of disease. Mechanical testing of materials is routinely performed in material engineering, but these techniques are not well suited for noninvasive, in vivo characterization of tissue.

There are several parameters that are used to characterize the mechanical properties of tissue including indices of shear, Young's and bulk moduli, nonlinearity, Poisson's ratio, viscosity, poroelastic parameters, anisotropy, and heterogeneity [24]. In engineering terms, the tissue property assessed by palpation is the elastic modulus (μ), a parameter that describes the relationship between stress and strain in a material. The elastic modulus quantifies an object's ability to resist deformation and is therefore a measure of rigidity or stiffness. The shear modulus (G) defines a material's resistance to deformation by shearing. The Young's modulus (E) is a material's resistance to deformation in extension. For biological tissue which is assumed to conserve volume under deformation (Poisson's ratio = 0.5), the shear and Young's moduli are proportional and the relationship is described by the equation: $G = E/3$. The bulk modulus (K) defines a material's resistance to compression. In tissue, the velocity of compression waves is very high, on the order of 1540 m/s and does not vary significant for different tissues compared to a shear wave velocity of 10 m/s, which has significant variations throughout the body [1]. Therefore, the shear modulus rather than the bulk modulus is preferable for the characterization of tissue.

Tissue is considered to be viscoelastic due to its characteristics of reversible deformation and viscous dissipation [25]. Viscoelastic materials exhibit both attenuating and dispersive characteristics. In elastography, mechanical properties are typically measured under dynamic conditions and are therefore characterized by a complex shear modulus $G^* = G' + iG''$ where G' and G'' are the storage and loss moduli respectively. The storage modulus (G') is a measure of the tissue's elastic behavior or its ability to store elastic energy. The loss modulus (G'') is related to the viscosity, or the tissue's ability to dissipate energy. If two parameters that describe the mechanical properties of tissue are calculated, the rest can be determined. In MRE, the shear modulus is quantified using a novel MRI-based technique.

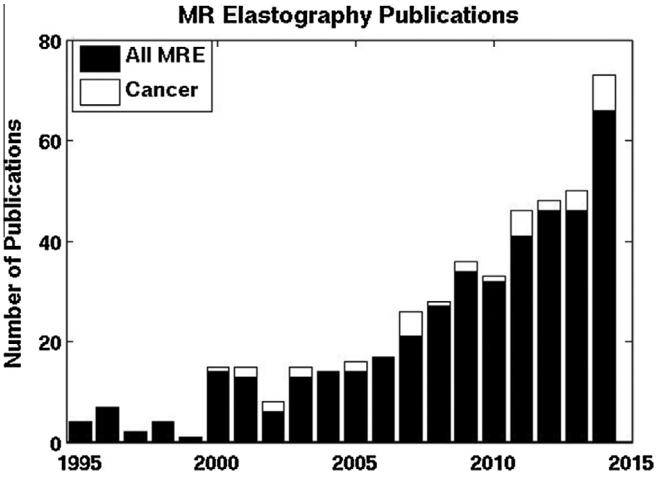

Fig. 1. A summary of a literature search on the topic of magnetic resonance elastography. These results are subdivided into two categories based on topic: cancer related and non-cancer related.

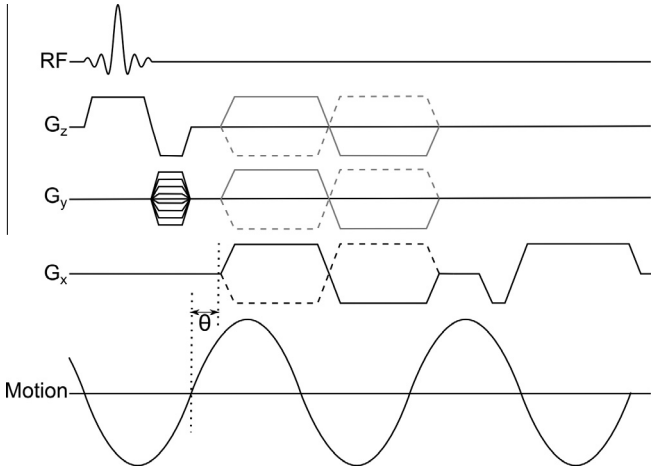

Fig. 2. Pulse sequence diagram for a gradient-recalled echo MRE pulse sequence. Sensitivity to tissue motion is achieved by adding bipolar motion-encoding gradients (MEGs) that are synchronized to the applied motion in the x, y, or z directions. The positive (solid line) and negative (dotted line) MEGs are used for phase-contrast imaging. A temporal relationship between tissue motion and the MEGs is achieved by varying the phase offset (θ).

2.2. MRE methodology

Elastography can be simply described by three steps: deforming the tissue of interest through application of mechanical waves, imaging the subsequent deformation, and calculating the corresponding mechanical properties.

2.2.1. Induced tissue deformation

The first step in quantitative elastography is to apply a stress to deform the tissue of interest. The deformation can be static or dynamic and can be from an internal source such as heart motion, pulsation of blood vessels, or an external mechanical source. In general elastography techniques are characterized by the temporal behavior of the stimulus. Static or quasistatic elastography is analogous to manual palpation with a frequency of 0–1 Hz while dynamic or harmonic techniques generate shear or longitudinal waves in the acoustic range (20–500 Hz) for in vivo applications. To produce low frequency shear waves in vivo, several external vibration sources have been used including electromechanical voice coils, piezoelectric bending elements, and pneumatically powered actuators [26,27]. Shear waves propagate through the tissue and produce displacements on the order of microns that are well within the safety limits set by the occupational safety standards of the European Union [28]. These low amplitude vibrations are well tolerated in all applications.

Shear wave motion produced by low frequency deformation is the basis for the quantification of tissue elasticity with MRE. Shear waves result in tissue motion perpendicular to the direction of wave propagation and are produced by drivers that oscillate parallel to the tissue surface. The speed of shear wave propagation is directly related to the mechanical properties of the tissue and is reflected in the wavelength. One limitation of this approach is the rapid attenuation of shear waves in soft tissue [29]. Minimally-attenuating longitudinal waves or compressional waves are produced with drivers oscillating perpendicular to the tissue surface and result in motion in the same direction as the wave propagation. While longitudinal waves have the advantage of low attenuation in tissue, the wave speed is on the order of 1540 m/s,

compared to 1–10 m/s for shear waves, making the former impractical or impossible to image with current techniques [1,30]. Shear waves can be created from longitudinal waves via the phenomenon of mode conversion at the interface between two dissimilar tissues [31]. High frequency longitudinal waves with mode conversion can be used to detect stiff lesions due to the differential attenuation of shear waves in stiff and soft material [31]. This technique may also be useful for deep seated tissues that are difficult to investigate using conventional low frequency elastography due to shear wave attenuation (see Fig. 1).

2.2.2. Measurement of tissue response to applied stress

The second and most critical step in elastography is to image the tissue response to the applied stress and measure either tissue displacement or velocity. There are numerous techniques to measure response including optical techniques, mechanical methods (pressure sensors, accelerometers), ultrasound, and MRI. The general principle is to encode the tissue deformation using different physical principles to eventually calculate the viscoelastic properties. In MRE, tissue displacement due to shear wave propagation is encoded in the phase of the magnetization by a modified phase-contrast pulse sequence with cyclic motion-encoding gradients (MEGs) (Fig. 2). The applied shear wave motion is synchronized with the MEGs in the *x*, *y*, or *z* directions to make the sequence sensitive to small amplitude tissue displacements. A temporal relationship can be acquired by varying the phase offset (θ) between the applied shear wave frequency and the oscillating MEGs at 3–8 evenly spaced time points [32]. The amplitude of tissue motion is recorded in the phase of the magnetization by the following equation:

$$\phi(\vec{r},\theta) = \frac{\gamma NT(\vec{G}\cdot\vec{\xi_0})}{2}\cos(\vec{k}\cdot\vec{r}+\theta) \quad (1)$$

where $\vec{r}$ is the position vector, θ is the phase offset between applied motion and the MEG, γ is the gyromagnetic ratio of protons in tissue ($\gamma/2\pi$ = 4257 Hz/G), N is the number of gradient pairs, T is the period of the MEG, G is the gradient amplitude, ξ_0 is the peak amplitude of motion, and k is the wave number [3]. The recorded phase of harmonic vibration is directly proportional to the physical displacement of the tissue. By measuring the phase over a full period of motion ($\theta = [0, 2\pi]$), one can relate the peak phase amplitude to the maximum displacement amplitude in the direction of the MEG (ξ) by the equation $\max\{\phi(\vec{r},\theta)\} = \gamma NTG\xi/2$. Therefore, the proportionality between the maximum phase and the maximum displacement is thus $\gamma NTG/2$. Typically two complementary phase measurements are obtained by reversing the polarity of the MEG and a phase difference image is calculated by subtraction or division in order to remove static phase errors due to B_0 inhomogeneity. The resulting phase or wave image captures one moment in time depicting the phase shift ($\phi(\vec{r},\theta)$) caused by the propagating wave. MRE is very sensitive to small displacements and is capable of detecting motion on the order of a few hundreds of nanometers [33].

Cyclic motion-encoding gradients can be incorporated in a variety of pulse sequences, and motion has been recorded using modified 2-D or 3-D gradient-echo (GRE), spin-echo (SE), echo-planar imaging (EPI), balanced steady-state free precession (bSSFP), spiral, and stimulated-echo pulse sequences [34]. Clinical applications of MRE in the liver typically use a GRE MRE sequence whereas SE or EPI sequences are used at higher magnetic fields due to requirements imposed by shorter T_2, inhomogeneous B_0, and limited signal-to-noise ratios [20]. Mechanical properties are not dependent on the magnetic field strength and preliminary studies have shown good reproducibility across systems from different manufacturers [35].

2.2.3. Calculation of corresponding mechanical properties

Quantitative maps of tissue stiffness, typically referred to as elastograms, are created by applying mathematical inversion algorithms to the recorded phase data. Elastic properties of tissue can be calculated from the phase data using the equations of motion that describe wave propagation within a medium [3,36]. Several simplifying assumptions are made, including that tissue can be modeled as an isotropic, linearly elastic, and locally homogeneous viscoelastic material. With these assumptions, the equation for harmonic motion is:

$$\mu\nabla^2\vec{U}(\vec{r},f) + (\lambda+\mu)\nabla(\nabla\cdot\vec{U}(\vec{r},f)) = -\rho\omega^2\vec{U}(\vec{r},f) \quad (2)$$

where μ and λ are the two Lamé constants describing the shear and longitudinal strain, measures of tissue deformation due to shear wave and longitudinal wave propagation, $U(\vec{r},f)$ is the vector displacement of the material at the position $\vec{r}$, ρ is the density of the material (1000 kg/m^3), and $\omega = 2\pi f, f$ is the frequency of the applied harmonic motion. Equation (2) can be simplified by assuming incompressibility ($\nabla\cdot\vec{U}(\vec{r},f) = 0$) and the equation simplifies to the Helmholtz equation:

$$\mu\nabla^2\vec{U}(\vec{r},f) = -\rho\omega^2\vec{U}(\vec{r},f) \quad (3)$$

With additional assumptions including negligible shear wave attenuation, the shear wave speed (v_s) is a function of the applied mechanical frequency (f_{app}) and the wavelength (λ_{sp}) or spatial frequency (f_{sp}) [32].

$$\mu = \rho\frac{f_{app}^2}{f_{sp}^2} = \rho v_s^2 = \rho(\lambda_{sp}f)^2 \quad (4)$$

Because of the relationship between the shear modulus and the spatial wavelength, the first data analysis methods for MRE manually measured the shear wavelength to determine tissue elasticity. Wave speed alone has been reported as an effective measure of shear modulus; however this will provide an inaccurate shear modulus in any tissue that is not purely elastic (i.e., that has no viscous component) [30]. Extensive work has been done to obtain an accurate estimation of tissue elasticity from the measured shear wave.

One of the most frequently used methods for reconstructing the mechanical properties of tissue is local frequency estimation (LFE). This technique estimates the spatial frequencies of an image and is a robust method for calculating the shear modulus from a single image (i.e., one sensitization direction and a single phase offset) [32,37]. LFE is relatively insensitive to noise and can be extended to three dimensions but has limited spatial resolution. An alternative to LFE with improved resolution is the phase gradient (PG), a calculation of the shear stiffness using the gradient of the phase of the first harmonic of the wave image. While PG has improved spatial resolution over LFE, it is very sensitive to noise and boundary conditions and will produce inaccurate results in the presence of interfering waves [32,38]. The complex shear modulus can be calculated by a direct inversion (DI) of the Helmholtz equation (Eq. (3)) [32,39–41]. Contrary to LFE and PG which assume an isotropic, linearly elastic, and locally homogeneous viscoelastic material, DI algorithms can include viscosity, anisotropy, and geometric effects [42]. DI methods may have higher spatial resolution than LFE but are sensitive to noise and low SNR due to the calculation of higher order derivatives.

Alternative approaches for reconstruction of viscoelastic properties have been developed that do not involve directly solving the differential equation of motion. These techniques include variational methods which incorporate data models to minimize the number of derivatives on noisy data [12,40,43] and finite element modeling (FEM) inversions. In this case, a model is created based

on the tissue geometry, boundary conditions, imaged displacement due to shear wave propagation, and an initial guess on the mechanical properties of tissue [44–47]. These inversions can be very robust to noise due to limited application of derivatives; however an accurate model is difficult in most applications and these methods may be computationally intensive [34].

2.3. Limitations and main sources of error

There are many technical and theoretical challenges for MRE applications in cancer that must be addressed before routine clinical use of this technique. The most significant limitation for MRE in cancer is spatial resolution. Depending on the inversion technique used to reconstruct the mechanical properties, elastograms can theoretically have a maximum of one half the resolution of the original MR image in a homogeneous material in the absence of noise, and in practice typically have one-third to one-fifth of the resolution [26]. Resolution of MRE is related to the shear wavelength in tissue: the shorter the wavelength, the higher the resolution. However, to achieve a shorter wavelength, high frequency shear waves must be applied at the expense of greater attenuation in tissue.

While the widely-used LFE inversion algorithm has proven to be a robust technique, its limited spatial resolution is a significant drawback in focal lesions. The LFE estimate of mechanical properties is blurred at sharp boundaries, i.e. the boundary between tumor and normal tissue, and an accurate stiffness estimate requires a minimum of one half wavelength [32]. This can be a significant limitation for small focal lesions. If the tumor diameter is approximately equal to one-eighth of the shear wavelength, the LFE estimate will never achieve the correct shear stiffness value; however the tumor will still be visible as a region of increased stiffness on the elastogram [32]. Inaccurate results may also occur with a two-dimensional wave inversion because any wave propagation at an angle to the imaging plane is not accounted for in the inversion, leading to an over- or under-estimation of stiffness. Similarly, wave reflection at tissue interfaces may also yield incorrect results. Application of 3D MRE may provide more accurate estimates of the mechanical properties of tissue and more work is need to decrease acquisition time and develop 3D reconstruction algorithms that incorporate complex boundary conditions, tissue anisotropy, nonlinearity, and viscoelastic characteristics.

While several unresolved challenges remain, significant progress has been made to increase the breadth of MRE applications in cancer. Several techniques to improve MRE spatial resolution through the application of higher frequency shear waves have been investigated, including using mode conversion from minimally attenuating, high frequency longitudinal waves and anatomy-specific mechanical actuators such as intracavity drivers for prostate MRE. Many of the issues related to reliability of MRE have been addressed in the liver, and several studies have shown that MRE has excellent reproducibility [48,49] and repeatability [50–52], high interobserver agreement [48,49], and reproducibility across different manufacturers [53].

3. The role of MRE in the study of cancer

3.1. Elasticity of cancer cells

Cancer, according to the National Institute of Heath, is defined as "the uncontrolled growth of abnormal cells in the human body." Abnormal cells have undergone genetic and epigenetic alterations that are reflected in various cellular functions including growth, apoptosis, motility, metabolism, signaling and remodeling [54]. Mounting evidence suggests that changes in the mechanical phenotype of cells occur with the development of cancer, including changes to cell structure, morphology, and responses to mechanical stimuli [22,55]. Cancer cells are generally softer and more deformable (i.e., have a lower elastic modulus) than normal cells, most likely due to organization of the cytoskeleton [56]. The reported elasticity of healthy human cells ranges from 0.75 (normal breast cell)[57] to 90 kPa (white blood cell). Despite the variability in normal cell stiffness, cancer cells have very low elasticity values (0.05–3.0 kPa), irrespective of cell tissue type [55]. While the cellular characteristics of malignancy have been extensively investigated, recent evidence suggests the role of the microenvironment in malignant transformation.

3.2. Elasticity of the tumor microenvironment

Although individual cancer cells are generally softer and more compliant than normal, healthy cells, tumors are typically stiffer than the surrounding healthy tissue. Cancer cells may occupy less than half the volume of a tumor; the remaining space is comprised of vasculature and interstitial stroma [58]. There are several factors that may contribute to the overall increased tumor stiffness, including tissue composition, increased collagen deposition, high cellularity, abnormal perfusion, altered vasculature, and higher interstitial pressure. Malignant neoplasms are usually associated with desmoplasia – the growth of fibrous or connective tissue from the deposition of extracellular matrix (ECM) [54]. The stromal reaction in cancer is similar to the reaction induced following an injury, i.e., increased ECM and growth factor production as well as scar formation, and cancer is often referred to as 'the wound that does not heal' [59,60].

The ECM in particular plays an important role in the development of cancer and overall structural characteristics of the tumor [61]. Comprised of proteins, glycoproteins, proteoglycans, and polysaccharides, the diverse ECM components create a unique structurally and functionally diverse environment. The ECM affects physical, biochemical, and biomechanical properties and increased ECM rigidity has been shown to promote the spread of malignant cancer cells [61]. High tumor interstitial pressure is an additional contributing factor to increased tumor stiffness and is most likely caused by microvascular pressure, abnormal flow and leaky lymph and blood vessels, and increased osmotic pressure of the interstitial space [62–64]. For example, the interstitial pressure in normal breast tissue has been reported as 0 mmHg compared to 15 mmHg in a solid breast tumor [58]. In addition to leaky vasculature, increased vessel density, including function and non-functional vessels, influences tumor mechanical properties [65].

3.3. Elasticity in oncology

In oncology, the mechanical properties of tissue play a significant role in the development, progression, and treatment of the disease. For example, in the liver, the presence of cirrhosis is a predisposing factor for the development of hepatocellular carcinoma (HCC) [66]; in 80–90% of cases, HCC develops in patients with cirrhosis [67]. In the prostate, elevated collagen deposition in malignant stromal cells was shown to be correlated to tumor grade, and collagen levels in the surrounding normal tissue may be a biomarker for patient survival [68–71]. Tumor stroma is emerging as a target for cancer therapy [72] and new imaging techniques will be critical for assessing response to therapy. High tumor interstitial pressure is a contributing factor to increased tumor stiffness and has been shown to be a barrier for the delivery of anti-cancer drugs [58,62]. A decrease in tumor interstitial pressure may be a biomarker of response to therapy [73], and reduction of tumor interstitial pressure improves the delivery of anti-cancer drugs [64]. There are many factors that contribute to altered tissue mechanical

Table 1
Sensitivity and specificity of breast cancer detection techniques.

Technique	Sensitivity (%)	Specificity (%)	Reference
Mammography	40	95	Kriege et al. (2004)
Ultrasound elastography	99	87	Barr et al. [86]
MRI alone	71	90	Kriege et al. (2004)
CE-MRI alone	90	75	Siegmann et al.
MRE + CE-MRI	90	90	[97]
CE-MRI alone	100	40	Sinkus et al. [96]
MRE + CE-MRI	100	60	

properties in cancer, and MRE may be a useful technique for the diagnosis of cancer and investigation of the mechanisms underlying malignant transformation and cancer progression.

4. Applications

4.1. Breast

In the detection of breast cancer, the breast self-exam is an effective and early screening tool in which the inherent differences in tissue stiffness between normal and malignant tissues are detected by means of manual palpation [2]. While palpation is widely used for routine breast screening as malignant masses are known to be stiffer than benign lesions and normal breast tissue [74,75], it lacks great sensitivity and specificity as a diagnostic test. MRE is well suited for breast cancer diagnosis and staging as a means to quantify the properties currently assessed by manual palpation.

The American Cancer Society recommendations include a clinical breast examination every 3 years for women aged 20–39, and every year including a mammogram for women over the age of 40 (ACS, Breast Cancer Facts & Figures 2011–2012, American Cancer Society, Inc. Atlanta). Early diagnosis has played a critical role in improving the 5-year relative survival of localized breast disease to 99% [76]. According to the National Cancer Institute, the overall sensitivity of mammography is 79%, but is lower in younger women (Table 1). Contrast-enhanced MRI (CE-MRI) is used for the detection and characterization of malignant lesions. CE-MRI is particularly useful in patients with dense breast parenchyma for whom mammography and ultrasound have reduced sensitivity for cancer detection [77]. Although MR imaging has high sensitivity (94–100%), accurate breast cancer diagnosis remains an ongoing clinical challenge due to the low or moderate specificity (37–97%) resulting in a large number of false-positive results [78,79]. Elimination of unnecessary biopsies is critical to reduce the emotional stress to the patient and financial burden to the healthcare system [80]. MRE is emerging as a complementary imaging tool because of its ability to address limitations in existing diagnostic imaging techniques.

Several novel imaging techniques have been applied to breast cancer screening with mixed results. Diffusion-weighted MRI and MR spectroscopy can potentially improve the accuracy of breast cancer imaging. Each has several potential pitfalls, however, including low spatial resolution and significant overlap in ADC cut-off values between malignant and benign lesions [81]. Recent work using ultrasound elastography techniques demonstrated improved accuracy of breast cancer diagnosis by inclusion of tumor shear strain or shear stiffness measurements [82–85]. One multicenter study by Barr et al. found a sensitivity of 99% and specificity of 87% for distinguishing between malignant and benign breast lesions using elastography (Table 1) [86]. While these studies show very encouraging results, ultrasound elastography techniques have several limitations, including the difficulty of imaging deep tissue and dense breast parenchyma, highly operator-dependent measurements, and the difficulty of distinguishing between benign breast lesions such as fibroadenomas and fibrocystic changes [87–89]. These limitations can result in poor image quality and low sensitivity (as low as 56.8%) [89]. Preliminary studies with MRE have demonstrated the potential of MRE to improve the accuracy and increase the diagnostic specificity of breast cancer MR imaging.

4.1.1. Elasticity of normal breast tissue

To measure the elastic properties of the breast by MRE, shear waves are first introduced into the breast (Fig. 3). The majority of MRE studies have been performed using a driver in contact with the breast and involve a slight precompression to provide a good coupling between driver and tissue with vibration frequencies ranging from 40 to 100 Hz. The first results of in vivo breast MRE characterized the properties of healthy tissue in 9 volunteers. The mean shear stiffness of glandular tissue was found to be higher than for adipose tissue (2.45 ± 0.2 kPa and 0.43 ± 0.07 kPa, respectively). Lorenzen et al. investigated the relationship between breast parenchyma elasticity and the menstrual cycle [90]. The elasticity of normal breast fibroglandular adipose tissue was monitored weekly over the course of 2 menstrual cycles in 5 volunteers using a slightly compressive transducer oscillating at a frequency of 65 Hz. Elasticity varied significantly and with a repeating pattern in all volunteers; the median value for fibroglandular tissue elasticity decreased significantly after 5 days of the onset of menses (−29%, $P = 0.010$) and reached the highest values during days 11–23 (+35%, $P = 0.028$). The cyclic change of breast tissue elasticity may have important implications in breast cancer if a ratio of tumor stiffness to normal tissue is used for diagnosis.

4.1.2. MRE to improve breast cancer specificity

The first published study of in vivo breast cancer MRE showed that malignant carcinomas were approximately 4 times stiffer than

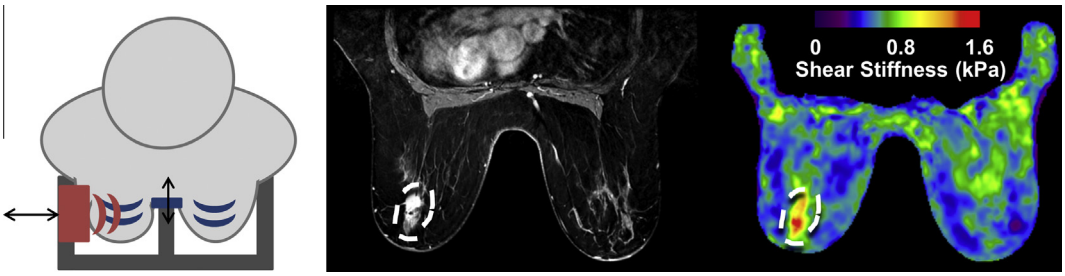

Fig. 3. MRE of breast cancer. Schematic of typical breast MRE setup showing two driving techniques (left). The double arrow shows the direction of oscillation for a compressive driver (red) and noncompressive driver (blue). Dynamic contrast-enhanced image (middle) and stiffness map (right) of an invasive lobular carcinoma of the left breast. Shear stiffness of the tumor was 1.25 kPa and the surrounding parenchyma was 0.46 kPa and 0.75 kPa for adipose and fibroglandular tissue respectively. The right (unaffected) breast global stiffness was 0.57 kPa. (Courtesy of Jun Chen, Mayo Clinic, Rochester, MN).

Table 2
MRE of breast cancer.

Reference	Tissue type	Shear modulus (kPa)	Loss modulus (kPa)	Study details	
				N	Frequency (Hz)
Normal volunteers					
McKnight et al. [91]	Fibroglandular	7.5 ± 3.6	–	6	100
	Adipose	3.3 ± 1.9			
Lorenzen et al. [92]	Breast Parenchyma	2.5	–	15	65
	Fatty breast tissue	1.7			
Benign breast disease					
Lorenzen et al. [92]	Benign Lesions	7.0	–	5	65
Xydeas et al. [95]	Fibroadenoma	1.4 ± 0.8	1.7 ± 0.8	11	65
	Fibrocystic changes	1.7 ± 0.8	1.0 ± 0.3		
	Normal Surrounding	1.2			
Sinkus et al. [93]	Fibroadenoma	2.6 ± 0.7	2.4 ± 1.9	1	65
	Normal Surrounding	0.36 ± 0.02			
Sinkus et al. [93]	Fibroadenoma	2.9 ± 0.3	2.7 ± 1.7	6	65
	Mastopathy	1.2 ± 0.5	0.8 ± 0.3	3	
	Normal Surrounding	0.87 ± 0.15			
Malignant breast disease					
McKnight et al. [91]	Breast Carcinoma	33 Range: 18–94	–	6	100
	Normal surrounding	8 Range: 4–16	–		
Lorenzen et al. [92]	Invasive breast tumor	15.9 Range: 8–28	–	15	65
Sinkus et al. [11]	Breast Carcinoma	3.5	–	1	65
	Normal surrounding	0.5–1			
Xydeas et al. [95]	Malignant lesions	3.1 ± 0.7	2.1 ± 1.2	5	65
	Normal surrounding	1.2 ± 0.2	1.0 ± 0.3		
Sinkus et al. [93]	Invasive ductal carcinoma	5.8 ± 1.2	3.0 ± 0.8	1	65
	Normal surrounding	1.1 ± 0.5	1.2 ± 0.8		
Sinkus et al. [93]	Breast Carcinoma	2.9 ± 0.3	2.4 ± 1.7	6	65

the surrounding normal fibroglandular tissue (Table 2) [91]. McKnight et al. [91] measured the shear stiffness in fibroglandular and adipose tissue in 6 healthy volunteers and tumor shear stiffness in 5 patients with infiltrating ductal carcinoma and 1 patient with infiltrating lobular carcinoma. Shear waves were applied at a frequency of 100 Hz using an electromechanical driver and contact plates on the medial and lateral aspect of the breast. In the normal volunteers, fibroglandular tissue had slightly higher shear elasticity values than adipose tissue (7.5 ± 3.6 kPa and 3.3 ± 1.9 kPa, respectively). The mean shear stiffness of the carcinomas was 33 kPa (range: 18–94 kPa), and shear stiffness of adipose tissue was increased from normal in the regions surrounding the tumor. Another preliminary study found that malignant lesions are significantly stiffer than benign lesions, normal breast parenchyma, and adipose tissue but that there is an overlap in the shear elasticity ranges of soft malignant tumors and stiff benign lesions. Lorenzen et al. investigated the potential of MRE to improve breast cancer diagnosis in 15 healthy volunteers, 15 patients with malignant tumors and 5 patients with benign lesions [92]. In this investigation, a transducer was positioned to slightly compress the breast tissue and apply mechanical waves at a frequency of 65 Hz. Normal breast tissue was found to have the lowest values of elasticity, including breast parenchyma (median: 2.5 kPa) and fatty breast tissue (median: 1.7 kPa). Benign breast lesions were found to be slightly stiffer (median: 7.0 kPa) than normal tissue and were significantly different from malignant tumors which had a median stiffness of 15.9 kPa (range: 8–28 kPa, $p = 0.0012$). While these feasibility studies had several limitations, including small sample size, the initial results were highly encouraging and motivated further development of MRE techniques to improve the diagnostic accuracy of breast cancer imaging.

Sinkus et al. devised a new technique for imaging the anisotropic and viscous properties of breast tissue in order to improve the specificity of breast cancer diagnosis [93]. Tissue was previously considered to be an isotropic material for the purposes of MRE reconstruction algorithms; however breast tissue in particular is known to be anisotropic. [74]. Additional information about the anisotropy of the breast lesion may provide complementary information to the elasticity for accurate diagnosis. The analysis technique presented uses a transversely isotropic model for reconstruction of the viscoelastic parameters to measure the eigenvalues of the elasticity tensor. The resulting viscoelastic tissue properties are described by the shear modulus μ, anisotropy τ, and shear viscosity ζ. In one example examining an invasive ductal carcinoma, the tumor displayed a markedly enhanced elasticity ($\mu^{\text{tumor}} = 5.8$ kPa; $\mu^{\text{normal}} = 1.1$ kPa) as well as increased anisotropy and viscosity ($\tau^{\text{tumor}} = 6.8$ kPa and $\zeta^{\text{tumor}} = 3.0$ kPa s compared to $\tau^{\text{normal}} = 0.9$ kPa and $\zeta^{\text{normal}} = 1.2$ Pa s). Further application of this technique in 15 patients produced similar results [94]. Malignant tumors were 2.2 times stiffer than benign lesions, and 3.3 times stiffer than the surrounding normal tissue. In this study, the mathematical curl operator was applied to the measured displacement field from the *x*, *y*, and *z* motion-encoding directions in order to remove any compressional waves which would otherwise contribute to a significant bias in the reconstructed viscoelastic properties. These results further support the potential of viscoelastic tissue properties measured by MRE for the accurate separation between malignant and benign lesions in the breast.

Xydeas et al. investigated the correlation between signal intensity and viscoelastic properties in 20 patients (11 benign, 5 malignant, and 4 with palpable lumps but nothing visible on contrast-enhanced MRI) [95]. A comparison of the shear modulus and shear viscosity of breast tumors showed that the shear modulus provided a good separation between malignant and benign lesions ($P < 0.004$ for fibroadenomas, $P < 0.04$ for fibrocystic changes) and malignant and normal breast tissue ($P < 0.0005$). Shear viscosity could not be used to distinguish between tissue types; however, the reported range in shear modulus overlapped for benign ($\leqslant$2.6 kPa) and malignant lesions ($\geqslant$2.4 kPa), indicating that elasticity alone cannot provide an accurate diagnosis. Similarly, morphologic characteristics, signal intensity data, and dynamic enhancement parameters from clinical MR imaging

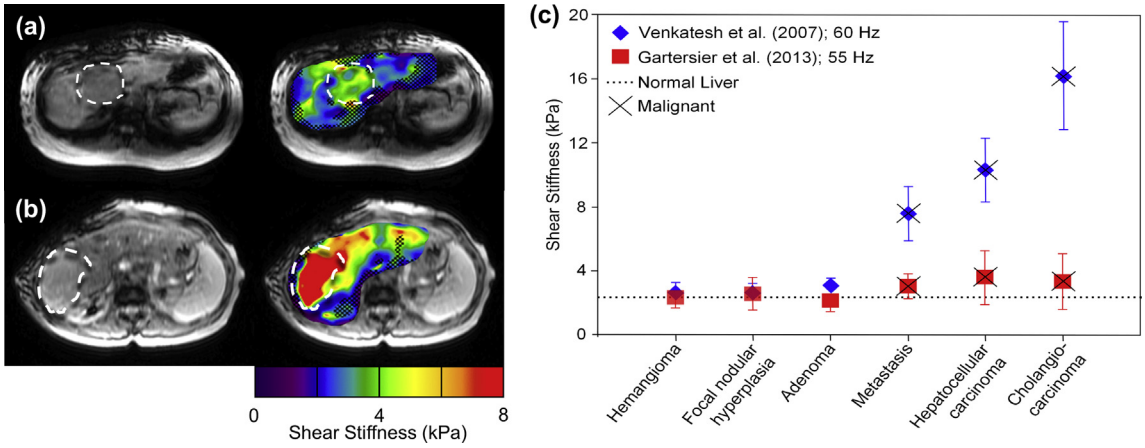

Fig. 4. MRE of liver cancer. T2-weighted image and corresponding elastograms for a benign (a) and malignant (b) liver tumor. (c) Mean shear stiffness and standard deviation reported for different liver tumor types as indicated. Malignant phenotypes are distinguished with an 'x' and mean shear stiffness for normal liver as reported by Venkatesh et al. is shown by the horizontal line. Mean shear stiffness of malignant tumors is significantly higher than benign lesions and normal liver.

protocols using a modified scoring system did not accurately separate malignant and benign lesions. Combining the modified breast MR imaging score and shear modulus yielded perfect separation between malignant and benign lesions. Despite several limitations, including small sample size and long acquisition times ($\geqslant$11 min), the results were very promising and encouraging for further investigation.

Two additional recent studies illustrated the capability of MRE to improve the specificity of contrast-enhanced MR mammography [96,97]. In an analysis of 68 patients (39 malignant, 29 benign), Sinkus et al. proposed a more sophisticated reconstruction algorithm to calculate the viscoelastic parameters in terms of a power law description, independent of any rheological model. Viscoelastic tissue properties are reported as the complex shear modulus $G^* = G_d + iG_l$, where G_d is the constant dynamic modulus and G_l is the linearly rising loss modulus, descriptors of the applied stress and resulting strain. MRE was performed over a range of frequencies between 65 and 100 Hz in one normal volunteer to observe the dispersion properties and frequency dependence of breast tissue. Ultimately, a frequency of 85 Hz was determined to be optimal in balancing low spatial resolution at low frequencies with high attenuation at high frequencies. CE-MRI alone had a sensitivity, specificity and area under the receiver operating characteristic curve AUC of 100%, 40% and 0.88, respectively, while MRE alone had an AUC of 0.91. An AUC of 0.96 was achieved by combining CE-MRI and MRE results, increasing the specificity from 40% to 60% with a sensitivity of 100%. A similar study by Siegmann et al. [97] evaluated the viscoelastic properties in 57 patients with lesions previously detected by palpation, mammography, ultrasound, or MRI. In this study, combining MRE and CE-MRI improved the diagnostic accuracy to an AUC = 0.96 compared to AUC = 0.93 by CE-MRI alone. These clinical and experimental observations show that inclusion of breast tumor viscoelasticity may contribute to improved diagnostic accuracy in the detection of breast cancer.

While MRI offers unique information regarding the extent of disease, staging, and recurrence, it is currently too expensive to replace mammography as a primary screening tool for the general population. For select individuals at high risk, the American Cancer Society recommends yearly screening with MRI. High risk is defined as having factors such as a known *BRAC1* or *BRAC2* gene mutation, a lifetime risk of breast cancer of 20–25% according to risk assessment tools based on family history, and/or those having had radiation therapy to the chest between the ages of 10 and 30 years [98]. MRE in combination with DCE-MRI may increase the diagnostic performance of breast MRI by increasing its specificity. Further investigations with larger cohorts will be required to validate these results.

4.2. Liver

Perhaps the most developed application of MRE is in the liver, where it has been used extensively to characterize liver parenchyma for both normal tissue and under different pathological states. An increasing number of studies have shown that MRE can be used to accurately and noninvasively diagnose liver fibrosis and cirrhosis [7,99–101] and has the potential to replace biopsy as standard of care. Liver MRE is safer, less expensive, and potentially more accurate than biopsy [20]. An important extension of hepatic MRE is for the detection and characterization of cancer. Although liver tumors are not typically found by palpation, one study showed that small tumors not detected preoperatively by imaging may be discovered through palpation by surgeons during laparotomy [102]. Elastography may therefore be useful in locating and characterizing hepatic tumors.

4.2.1. Elasticity of normal liver

Clinical hepatic MRE is typically performed at a frequency of 60 Hz using a pneumatic driver coupled to a rigid passive driver positioned over the liver. A modified GRE sequence with an MEG in the z direction (longitudinal axis of the body) is generally used for clinical hepatic applications. Typical sequence parameters include a repetition time (TR) of 50 ms, echo time (TE) 20 ms, 30–48 cm field of view, 256 $\times$ 64 image acquisition matrix, 4 phase offsets, BW = 33 kHz (bandwidth/pixel value), 6–10 mm slice thickness, and parallel imaging with acceleration factor 2 [49]. Normal liver tissue is fairly soft, with a reported mean shear stiffness of 2.05–2.44 kPa (range = 1.54–2.87 kPa) [103]. Several studies have been performed to assess the reliability of hepatic MRE measurements, and have found that MRE has excellent reproducibility [48,49] and repeatability [50–52].

4.2.2. Focal liver lesions

Focal liver tumors are detected and characterized clinically using morphological imaging approaches combined with additional information from contrast-enhanced and diffusion weighted sequences. These techniques are qualitative and, while highly sensitive for tumor detection, suffer from low specificity for distinguishing between malignant and benign lesions (Fig. 4). Preliminary studies have reported excellent accuracy of MRE in the noninvasive differentiation of malignant and benign solid liver

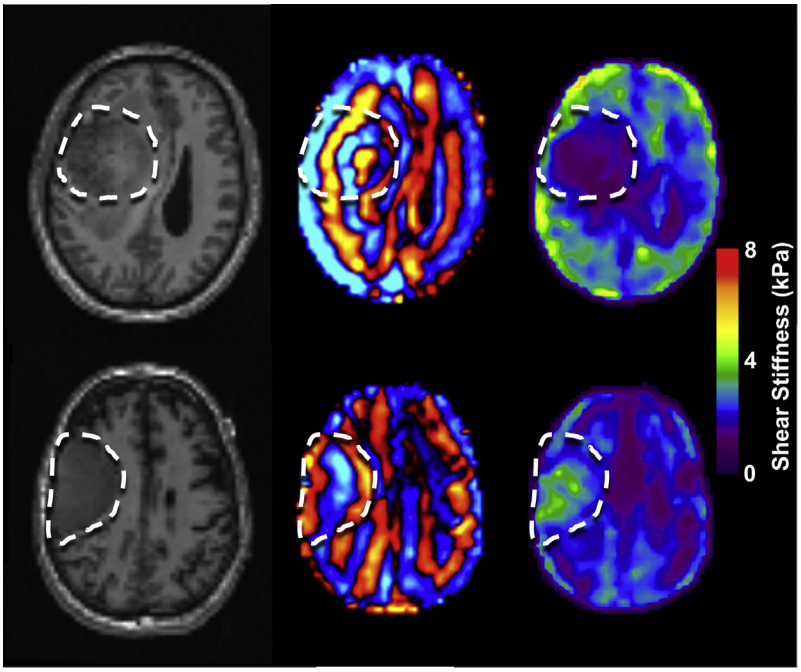

Fig. 5. MRE of brain cancer. T2-weighted anatomical images (left), wave images (middle) and elastograms (right) for two patients with meningiomas. The first patient (top row) had a significantly softer meningioma than the second (bottom row). Note that the shear wavelength in the first case is much shorter than in the second case.

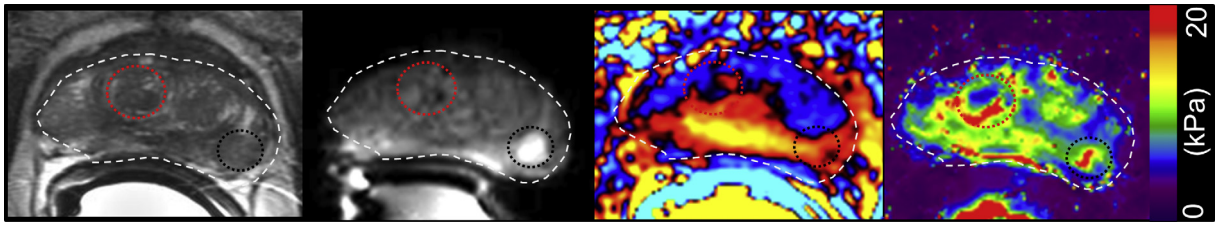

Fig. 6. MRE of prostate cancer. A T2-weighted image (first column), diffusion weighted image (b = 800 s/mm^2) (second column), wave image (third column), and elastograms (fourth column) acquired at 300 Hz of a subject diagnosed with prostate cancer. The black circle designates a region in the peripheral zone diagnosed as prostate cancer by a uroradiologist and corresponds to an area of elevated stiffness. The red circle indicates a low signal in the T2-weighted image corresponding to a ring of elevated stiffness in the elastograms in the right transition zone. The prostate boundary has been outlined with a white dashed line (Courtesy of Arvin Arani, Mayo Clinic, Rochester, MN and Rajiv Chopra, UT Southwestern Medical Center).

tumors. Venkatesh et al. [99] evaluated 44 solid liver tumors (13 benign and 31 malignant in 29 patients). Continuous acoustic vibrations at a frequency of 60 Hz were applied to the liver using a 19 cm passive driver and imaged using a gradient-echo MRE sequence. Elastograms were reconstructed using a local frequency estimation inversion algorithm. Mean shear stiffness of malignant tumors was significantly higher than for benign tumors and normal liver. The reported values were 10.1 kPa (range 6.2–19.6 kPa) for malignant tumors, 2.7 kPa (range 1.6–3.2 kPa) for benign tumors, and 2.3 kPa (range 1.8–2.8 kPa) for normal liver. A cutoff value of 5 kPa accurately separated malignant tumors from benign lesions and normal liver. The mean shear stiffness for benign tumors and normal liver parenchyma showed no significant difference. Garteiser et al. [104] evaluated 72 focal liver lesions (37 benign and 35 malignant in 94 patients) and calculated the complex shear modulus and its real and imaginary components, i.e., the storage and loss moduli. The absolute shear modulus and loss modulus were significantly higher in malignant tumors; however the storage modulus was not significantly different. The loss modulus was the dominating component of the complex shear modulus and more accurately discriminated malignant from benign lesions (2.25 ± 0.26 kPa vs. 1.05 ± 0.13 kPa respectively). A threshold of 1.38 kPa was recommended for discriminating between benign lesions using the loss modulus ($P < 0.001$). These studies suggest that MRE may be a promising biomarker for differentiating between benign and malignant focal liver lesions.

4.2.3. Hepatocellular carcinoma

Increased liver stiffness in the form of cirrhosis is a significant risk factor for the development of hepatocellular carcinoma (HCC) [66]. Patients with cirrhosis comprise 80–90% of cases of HCC [105], and HCC is the leading cause of death in this population [106]. As a result, current clinical recommendations include screening every 6–12 months for HCC in patients with cirrhosis. As cirrhosis is a risk factor for HCC and is characterized by late stage scarring or fibrosis of the liver, increased stiffness may correlate with the increased risk of HCC. Recent studies using transient elastography have shown that increased liver stiffness is associated with an increased risk of developing HCC [107]. One study by Motosugi et al. investigated liver stiffness of non-affected hepatic parenchyma in 30 patients with HCC compared to 60 age matched controls with compensated cirrhosis using MRE [108]. Mean shear stiffness of the unaffected hepatic parenchyma in HCC patients was 6.1 kPa compared to 6.3 kPa in the controls. No correlation between liver stiffness and presence of HCC was observed. These results conflict with an increasing number of studies using

transient elastography and the authors suggest that, while transient elastography is limited to measuring only a small fraction of the right lateral liver, MRE obtains a global estimate of hepatic stiffness. This volumetric difference in the quantification of liver stiffness may explain the conflicting results. Future studies are necessary to explore the role of increased hepatic stiffness in the development of hepatocellular carcinoma.

4.3. Brain

The application of MRE in the brain is an area of significant research and clinical interest due to the potential of altered mechanical properties of brain tissue in a variety of pathologies including cancer, Alzheimer's disease, hydrocephalus, and multiple sclerosis [109]. The feasibility of brain MRE is one of its principal advantages over ultrasound elastography which is hampered by the lack of an acoustic window through the skull. MR imaging is well established as the ideal modality to noninvasively assess brain morphology and function, and MRE of the brain is a natural extension to provide complementary information to existing techniques. The brain is protected and isolated by the skull; therefore prior to MRE very little was known about the mechanical properties of the brain in vivo. Significant work was conducted on ex vivo specimens and in animal models using MRE [110–113], but many factors contribute to tissue stiffness in vivo and it is not possible to make accurate comparisons with ex vivo samples. These early studies resulted in significant variations in the reported mechanical properties of the brain and even conflicting conclusions about whether white matter or gray matter is stiffer (Fig. 5). One of the significant technical challenges related to brain MRE is introducing shear waves into the brain. Several techniques have been utilized, including bite bars, rigid and soft passive actuators placed beneath the head, and devices that vibrate a cradle the head is resting in [10,27,114–118]. One of the first applications of brain MRE by Xu et al. used an actuator fixed to the head coil to induce vibrations at 100, 150, and 200 Hz in 3 volunteers [119]. Although no quantitative measurements were reported, the authors reported that the elastic modulus of white matter was higher than that of gray matter (see Fig. 6).

4.3.1. Elasticity of normal brain

In one of the earliest studies that quantified brain stiffness using MRE, Kruse et al. evaluated 25 healthy subjects (range 23–79 years) [114]. Shear waves at a frequency of 100 Hz were applied using a bite block and a 2D inversion using the LFE algorithm. Mean shear stiffness of white matter was higher than for gray matter (14.8 kPa vs. 5.22 kPa respectively, $p < 0.0001$). No apparent trend with respect to age of the volunteer was observed. The relationships between the mechanical properties of white matter and gray matter are still debated in the literature. The low elastic modulus of the brain can be explained by the almost complete lack of ECM that comprises most other soft tissues [120].

The viscoelastic properties of brain tissue can be characterized by the shear stiffness and shear viscosity. Sack et al. quantified these parameters in 6 volunteers [10]. A head rocker actuator was used to apply shear waves at 25 and 50 Hz and images were acquired using a single-shot spin-echo EPI MRE sequence. Tissue mechanical properties were calculated based on the Voight model of viscoelasticity and reported as a complex modulus ($G = G' + iG''$) where G' is the shear modulus or dynamic modulus and G'' is the loss modulus and describes the shear viscosity. The mean shear modulus at 25 and 50 Hz was 1.17 ± 0.03 kPa (range: 1.01–1.31 kPa) and 1.56 ± 0.07 kPa (range: 1.33–1.77 kPa). The shear modulus is approximately 1/3 higher at 50 Hz than at 25 Hz. The shear viscosity at 25 and 50 Hz was 3.1 ± 0.4 Pa s (range: 2.1–4.6 Pa.s) and 3.4 ± 0.2 Pa s (range: 2.5–4.2 Pa s) and did not vary significantly with frequency of excitation. The authors reported only global stiffness values due to geometric biases at the surface of the brain resulting from wave diffraction or other interference at the boundary between the brain and the skull. Green et al. found that gray matter had a higher mean value for the storage modulus than white matter (3.1 kPa vs. 2.7 kPa, $p = 0.02$) in 5 healthy subjects [115]. There was no significant difference in the loss modulus between the two tissues (2.5 kPa for both gray matter and white matter). In this case, a frequency of 90 Hz was applied using a bite bar, and 3D MRE processing techniques were used to create the elastograms. The authors suggest that low shear wave amplitude in the central regions of the brain may lead to inaccurate assessment of tissue mechanical properties.

Recent evidence suggests that the viscoelastic properties of the brain may be dependent on age and gender [116]. Sack et al. [116] investigated the brain viscoelasticity in 55 healthy volunteers (23 females) ranging from 18 to 88 years of age. Multi-frequency MRE was performed by applying four vibration frequencies ranging from 25 to 62.5 Hz using a head cradle. Brain elasticity and viscosity were calculated using a rheological springpot model and combined into two parameters μ and α to describe the solid-fluid behavior and microstructure of tissue. With age, the healthy adult brain was found to become more fluid-like, characterized by a decrease in μ of 0.8% per year ($P < 0.001$) with no apparent change in the microstructure α. On average, μ was 9% higher in age-matched female subjects compared to their male counterparts, suggesting a more solid-like brain tissue ($P = 0.016$). Guo et al. generated normalized maps of viscoelasticity in 23 healthy volunteers in an effort to create an elastographic atlas of brain anatomy [121]. Three-dimensional multifrequency MRE (3DMMRE) data were processed using a previously described multi-frequency dual elasto-visco (MDEV) reconstruction [122]. Spatially averaged, normalized MRE parameters were reported for four brain regions: white matter, thalamus, head of caudate nucleus, and the corpus callosum genu. Establishing normative values of brain stiffness is a critical step in the use of MRE for the evaluation of the mechanical properties of the brain in various physiological and pathological states.

4.3.2. Meningioma

An emerging application of brain MRE is in the preoperative assessment of the stiffness of meningiomas, a typically benign lesion that arises from the meninges (thin layers of tissue covering the brain and spinal cord) that have a diverse range of mechanical properties. The stiffness of a meningioma can have a significant effect on the surgical procedure, where a soft tumor is easily resected, while more fibrous, stiffer tumors often require longer surgerical procedures involving tedious and difficult dissections [123]. One study by Xu et al. [124] compared qualitative assessments of MRE wave data with intraoperative evaluation of tumor stiffness through the report from the neurosurgeon. Shear waves at a frequency of 150 Hz were induced using a bite bar. Tumor shear stiffness was evaluated with respect to white matter and found to be softer in one transitional meningioma, similar to white matter for two fibrous meningiomas, and stiffer for a schwannoma, hemangiopericytoma, and transitional meningioma. The preoperative MRE assessment of tumor stiffness agreed with the surgical assessment in all 6 cases. Murphy et al. [123] found that MRE can be used to preoperatively predict tumor consistency. In this prospective study, MRE was performed in 13 patients prior to surgery and a qualitative assessment of tumor stiffness was obtained by the neurosurgeon at the time of resection. MRE was performed in three dimensions at a frequency of 60 Hz using a soft "pillow-like" driver (Fig. 5). The authors suggested that it may be important to normalize tumor stiffness to the surrounding brain

tissue due to intra-subject variability in unaffected brain tissue mechanical properties. The normalized tumor stiffness (ratio of tumor stiffness to surrounding brain tissue stiffness) was significantly correlated with the intraoperative neurosurgeon's assessment ($p = 0.0032$).

4.3.3. Glioma

Gliomas are the most common type of primary brain tumor in adults. Glioma is a particularly devastating cancer with a median survival time of approximately 14.6 months. According to the American Brain Tumor Association, less than 30 percent of patients survive two years and less than 10 percent survive beyond five years. Conventional MR imaging is currently the gold standard for the diagnosis, pre-surgical planning, and post-therapeutic monitoring of gliomas. It is highly sensitive for tumor detection, but has low specificity for determination of tumor grade [125]. Biopsy is currently the clinical standard of care for the histological classification of glioma. MR imaging of gliomas is a very active area of research, aimed at improving the assessment of glioma morphology and functionality based on anatomical features and physiological parameters such as tumor blood flow, vascularity, permeability, and molecular markers. Although contrast enhancement is typically associated with malignancy, up to one-third of non-enhancing gliomas are malignant [125]. As part of a broader evaluation of the viscoelastic properties of intracranial tumors, Reiss-Zimmermann et al. quantified the magnitude $|G^*|$ and phase angle φ of the complex shear modulus in patients with glioblastoma (WHO grade IV, $n = 11$) and anaplastic astrocytoma (WHO grade III, $n = 3$) using three-dimensional multi-frequency MRE [126]. Glioblastomas had a large range of $|G^*|$ values and were slightly softer than WHO grade III tumors.

MRE has been successfully applied for the evaluation of the normal brain and cerebral pathologies including focal lesions, neurodegenerative disorders such as Alzheimer's disease, normal pressure hydrocephalus, multiple sclerosis, and progressive supranuclear palsy. Future applications may include the preoperative assessment of intracranial tumors such as pituitary adenoma, a common tumor of the pituitary gland with increased surgical risk related to the morphological and mechanical properties of the tumor [127]. While many technical challenges have been addressed for the implementation of brain MRE and reconstruction of viscoelastic parameters, several significant issues remain. Future investigations should include larger cohorts of patients to establish threshold and reference values for diagnostic purposes, evaluation of high-resolution techniques, and development of robust inversion techniques for the calculation of viscoelastic properties in nonlinear, anisotropic brain tissue with complex boundary conditions.

4.4. Prostate

With the implementation of new screening procedures, including the annual digital rectal examination and prostate-specific antigen based on recommendations from the American Cancer Society, an increasing number of cases of prostate cancer are being detected both in younger men and at earlier stages of the disease. Current diagnostic techniques, however, are unable to provide accurate spatial localization, resulting in treatment strategies including surgery and radiation therapy that target the entire prostate [128,129]. This over-treatment often leads to long-term morbidity and complications related to sexual, urinary, or rectal function [130]. There is an ongoing effort to develop more targeted therapies in prostate cancer that is hampered by the lack of techniques to reliably define the spatial distribution of cancer within the gland. Therefore, there is a critical need for a noninvasive technique for prostate cancer detection and spatial localization which can be used to identify locations for biopsy, improve specificity to reduce unnecessary biopsies, and provide opportunities for more targeted therapies. Improved imaging methods for prostate cancer localization and characterization would have a significant impact on clinical management of the disease in patients.

MRI has emerged as a promising technique for identification and localization of prostate cancer due to its excellent spatial resolution and tissue contrast. One strategy in particular has emerged as a promising diagnostic technique: multiparametric magnetic resonance imaging (MPMRI), which incorporates morphologic information from T2-weighted images, functional biochemical composition from MR spectroscopy, tissue magnetization relaxation, and tissue vascularization from DCE-MRI [131]. Tissue elasticity may provide complementary information to MPMRI to improve the identification, localization and staging of prostate cancer. Several ex vivo and in vitro studies have demonstrated that elasticity measurements can distinguish between malignant prostate cancer from benign disease and normal tissue. Individual malignant prostate stromal cells have increased collagen deposition compared to normal, and cancer grade may be directly proportional to the amount of collagen deposition [69–71]. These studies detail the importance of tissue elasticity in prostate cancer and suggest that structural and mechanical information may be useful for diagnosis and staging. Several studies have reported a 2–3 fold increase in stiffness in malignant tumors compared to normal tissue in excised prostate [68,74,132]. In order to evaluate prostate cancer elasticity in vivo, an important prerequisite is generation of shear waves with adequate amplitude and wavelength in this deep-seated organ.

4.4.1. Elasticity of normal prostate

Conventional MRE uses an external actuator to transmit shear waves into the tissue of interest. Kemper et al. used an external oscillator attached to the pelvic bone in 7 healthy volunteers to assess the technical feasibility of MRE of the prostate gland [133]. Reconstructed elasticity distributions correlated well with the zonal anatomy of the prostate gland, and mean shear stiffness of the central and peripheral portion was 2.2 ± 0.3 kPa and 3.3 ± 0.5 kPa respectively. Due to the rapid attenuation of high frequency shear waves in soft tissue, only frequencies below 65 Hz reached the prostate gland using an external driver. At this frequency, the corresponding wavelength was on the scale of the entire prostate, making it difficult to resolve small localized regions of increased stiffness corresponding to cancer. Prostate MRE has many significant technical challenges related to the transmission of shear waves with adequate amplitude and wavelengths to resolve localized increases in stiffness. An increasing number of studies have explored new ways of generating shear waves in the prostate.

4.4.2. Intracavity driver development for prostate MRE

To produce shear waves in the prostate with adequate propagation at a reasonable frequency, Chopra et al. designed a transurethral actuator [134]. A flexible tube with small holes ($\sim$1 mm) is inserted into the urethra and suction is used to create mechanical fixation of the tissue to the driver. The soft tube is connected to a rigid brass tube that is made to vibrate by a piezoceramic stack actuator. Initial experiments were performed in a both a homogeneous gel phantom and a phantom with regions of increased stiffness at frequencies of 150, 175, 200 and 250 Hz. The results of the phantom experiment demonstrated excellent performance and reproducibility with clearly visible radial waves propagating away from the transurethral driver. While the new driver was not tested in humans, a canine experiment demonstrated the feasibility of transurethral MRE in vivo where continuous, uniform shear waves were observed throughout the entire prostate gland. A transurethral actuator provides many advantages over external

drivers due to the proximity of the vibration source to the tissue of interest. Shear waves generated from the transurethral driver have a penetration depth of 3-5 cm as opposed to 15 cm for an external driver. The shorter penetration depth allows for higher frequencies of applied motion resulting in higher spatial resolution. The spatial and stiffness resolution of transurethral MRE was evaluated in an effort to determine if prostate MRE sensitivity is adequate for cancer detection [135]. In a prostate phantom, MRE could be used to identify increased regions of stiffness as small as 0.05 cm^3 in volume (0.4 cm in diameter) at a frequency of 200 Hz. A threshold of 0.5 cm^3 may be the lower limit of clinically significant tumors [136,137]. A frequency of 400 Hz was required to obtain shear stiffness measurements that matched the values obtained using mechanical compression testing in a 10 mm diameter inclusion. The initial results of MRE in the prostate using a transurethral driver are very encouraging, but the invasive nature of the driver may limit the clinical applications of this technique.

An alternative to the invasive transurethral driver was recently proposed by Arani et al. [135]. In an initial feasibility study, an endorectal coil was used to both generate shear waves and acquire images in the prostate [138]. Use of the endorectal coil was motivated by the current clinical use of the coil for MPMRI of the prostate which may facilitate the incorporation of elasticity information into MPMRI. The endorectal coil was mechanically coupled to a piezoceramic actuator. Initial experiments were performed in both a homogeneous prostate mimicking phantom and a phantom with stiff inclusions. This is the first publication that simultaneously imaged and applied shear waves using a 2D TR-interleaved imaging approach. The phantom results demonstrated uniform shear waves with no adverse effects on SNR due to the simultaneous acquisition. A subsequent study in 12 human volunteers tested the feasibility of incorporating endorectal MRE into MPMRI [139]. Shear waves were generated in the prostate using a rigid or an inflatable endorectal coil at 100, 200 and 300 Hz. Uniform shear wave propagation across the entire prostate was achieved in all volunteers and the vibrations were well tolerated. Mean shear stiffness at a frequency of 200 Hz was 9 ± 2 kPa for both the central gland and peripheral zone with a repeatability of ±38% and ±22% respectively. One volunteer was previously diagnosed with prostate cancer and a region of elevated stiffness was observed in the elastograms. The results of this study demonstrated the feasibility of using an endorectal coil for prostate MRE and future studies will determine whether prostate MRE can provide clinically useful information for multiparametric prostate MRI.

Another approach for prostate MRE utilizes a transperineal mechanical driver as an alternative to the more invasive endorectal and intraperitoneal actuators [140]. Transperineal excitation is achieved using a hydraulic system positioned between the legs over the undergarment and exerting a small compression on the perineum. To balance the shear wave attenuation at high frequencies and poor spatial resolution at long wavelengths, the study used a second harmonic acquisition where the frequency of the MEGs was twice the frequency of mechanical excitation (100 Hz and 50 Hz respectively). Phantom studies suggest that lesions as small as 0.5 cc can be resolved using the proposed method. This technique was evaluated in 6 healthy volunteers to measure mean prostate elasticity and to determine the repeatability. No discomfort or pain was reported. Mean shear stiffness of the prostate gland was 8.2 kPa (range = 6.7–9.6 kPa) and the coefficient of repeatability was 1.37 kPa. This study demonstrated the feasibility of using a noninvasive technique for prostate MRE with initial in vivo measurements.

4.4.3. Initial applications in prostate cancer

A more recent study of 10 healthy volunteers and 18 patients (8 with prostate cancer, 10 with prostatitis) by Li et al. achieved a frequency of 100 Hz in the prostate gland using a transducer placed above the pelvic bone [141]. This study showed that MRE can be used to distinguish between prostate cancer and benign prostatic disease. The mean shear stiffness and viscosity were significantly higher in prostate cancer (6.55 kPa and 6.56 Pa s) than in benign prostatitis (1.99 kPa and 2.13 Pa s; $p < 0.01$) and normal tissue (2.26 kPa and 2.38 Pa s; $p < 0.01$). Increased elasticity in prostate cancer also correlated with Gleason scores ($r = 0.913$, $p < 0.01$). This study found a good separation between malignant and benign prostate disease based on the viscoelasticity of tissue and motivates further investigation of MRE as a biomarker for prostate cancer.

In one study by Sahebjavaher et al., transperineal prostate MRE was evaluated in 11 patients and the resulting elasticity results were compared with histopathology data and Gleason score [142]. The coefficient of repeatability of in vivo transperineal prostate cancer MRE ranged from 4.8 to 9 kPa, corresponding to a 25% variation in stiffness. This is a significant limitation of this technique; future work is needed to improve repeatability. Tissue elasticity was quantified in several regions throughout the prostate including the prostate capsule, peripheral zone, central gland and transition zone. A statistically significant difference in mean elasticity from normal tissue was observed in cancerous tissue with a Gleason score of at least 3 + 3 ($p < 0.05$) with tumors in the peripheral (AUC = 0.72) and central zones (AUC = 0.67). Overall, MRE was able to diagnose prostate cancer with both a sensitivity and specificity of 0.63 and an AUC of 0.68. In this study, not all cancerous tissue was found to be stiffer than normal. This was the first published study to compare prostate cancer elasticity and histopathology; future investigation should focus on improving the repeatability and spatial resolution through application of higher frequency mechanical waves for clinical implementation of this technique.

MRE for prostate cancer diagnosis, spatial localization, and disease staging is an emerging application. Significant progress has been made in the development of various techniques for the generation of mechanical waves in the prostate gland. While there are significant limitations that need to be addressed before clinical implementation of this technique, including improved sensitivity, specificity and repeatability, initial results are encouraging and provide motivation for further research in this area.

4.5. Other organs

4.5.1. Thyroid

Significant progress has been made in the field of ultrasound elastography on using tissue elasticity to distinguish between malignant and benign lesions in the thyroid gland [143,144]. While the initial results are encouraging, there are several significant limitations of ultrasound elastography, such as the poor reproducibility due to the operator-dependent nature of this technique [145]. In the first investigation into the application of MRE in the thyroid gland, Bahn et al. developed and evaluated MRE for the diagnosis of thyroid disease [19]. Shear waves were introduced at frequencies of 80 and 100 Hz using an electromechanical transducer gently resting over the thyroid lobes. The mean shear stiffness of thyroid lobes containing a malignant nodule ($n = 2$) was not significantly different from lobes containing a benign nodule ($n = 8$) or normal volunteers ($n = 12$). The sensitivity of this technique to the differences in stiffness between malignant and benign lesions was likely significantly decreased by the use of the entire lobe containing the nodule as the region of interest. Improved resolution and use of an ROI corresponding to the isolated nodule may improve the sensitivity of MRE in the diagnosis of thyroid cancer.

Yeung et al. developed a novel driver design for MRE of the head and neck using a headrest mold and piston extension [118]. A

frequency of 50 Hz was used to measure the storage modulus (G') and loss modulus (G'') in the normal thyroid in six volunteers (G' = 0.58, G'' = 0.42), metastatic node in two patients (G' = 0.66, G'' = 0.58), and papillary carcinoma in one patient (G' = 0.17, G'' = 0.28). While this study demonstrated the successful implementation of a novel driver for head and neck MRE, the initial results suggest that malignant thyroid tumors are softer than normal tissue, contrary to the findings outlined in the previously described study. Both studies were limited by extremely small sample size (n = 1 and n = 2); therefore further studies are needed to evaluate MRE for the diagnosis of thyroid cancer.

4.5.2. Uterus

One study by Stewart et al. investigated the feasibility of using MRE to evaluate the stiffness of uterine leiomyomas [146]. These are often referred to as uterine fibroids due to the fact that they are typically stiffer than the surrounding myometrium and are characterized by the presence of excessive extracellular matrix [147]. MRE was performed in 6 patients with uterine leiomyomas using a 19 cm passive driver positioned over the lower abdomen to induce shear waves at a frequency of 60 Hz in the uterus. Data were acquired using a 2D gradient-recalled echo-based MRE and processed with a 2D LFE algorithm. Mean elasticity of the uterine leiomyomas was successfully quantified in all patients (range: 3.95–6.68 kPa). Variability in the elasticity of leiomyomas may have clinical significance for differentiating fibroids from rare uterine sarcomas. Currently, accurate diagnosis is difficult utilizing conventional imaging techniques; however increasing evidence from the breast, brain, liver and prostate suggests that MRE may be useful for distinguishing between malignant and benign lesions, and further investigation may support the use of MRE for the diagnosis and characterization of uterine neoplasms.

4.5.3. Pancreas

Compared to other cancers, pancreatic cancer is relatively rare. It is only the 12th most commonly diagnosed cancer in the United States, but it is a particularly devastating disease with a five year survival of only 6.7% [148]. Early diagnosis of pancreatic cancer would have a significant clinical impact on patient outcome; however, current imaging modalities have very poor sensitivity for the detection of pancreatic cancer [149]. A recent study by Shi et al. explored the feasibility of pancreatic MRE in 12 healthy volunteers using a soft passive driver placed in tight contact with the body to induce low frequency shear waves (40 and 60 Hz) deep into the abdomen [17]. A mechanical driving frequency of 40 Hz produced the most reliable results for pancreas MRE. Data were acquired using a multi-slice spin echo EPI MRE sequence and a 3D direct inversion algorithm was used to create the elastograms. Shear stiffness was quantified in the five pancreatic sub-regions: uncinate, head, neck, body and tail. Mean pancreatic stiffness was 1.15 ± 0.17 kPa and 2.09 ± 0.33 kPa for 40 and 60 Hz respectively. At 60 Hz pancreatic stiffness was found to be very similar to the liver stiffness. Establishing normative values of pancreatic stiffness is a critical first step in the use of MRE for the evaluation of pancreatic cancer. The current experimental design with a low frequency of 40 Hz will need to be evaluated to determine if the spatial resolution is adequate to resolve small regions of increased stiffness in a tumor.

4.5.4. Future applications

Thermal tumor ablation is an important noninvasive treatment for focal lesions. Medical imaging modalities are used to plan, guide, and monitor therapy, and MR imaging is uniquely suited to this task due to the excellent soft tissue contrast and sensitivity to temperature changes using MR thermometry. However, MR thermometry is limited in the evaluation of tissue ablation due to uncertainties in temperature estimates based on variable tissue conductivity, local blood flow or different tumor cellular sensitivity [150]. Accurate quantification of the spatial extent of ablation is critical for the success of this technique. Wu et al. showed that the tissue ablated by focused ultrasound was stiffer than normal tissue in ex vivo porcine tissue [151]. Le et al. demonstrated the feasibility of the simultaneous measurement of tissue temperature and stiffness using MR thermometry and MRE [152,153]. Chen et al. evaluated the feasibility of using MRE to monitor the extent of in vivo laser ablation in porcine liver [150]. Following lethal thermal dose ablation, tissue stiffness was significantly greater than baseline but was unchanged in sub-lethal thermal ablations. Further studies are required to assess the accuracy of MRE in monitoring thermal ablation and correlation to clinical outcome.

Significant progress has been made with MRE in a variety other organs including lung, heart, spleen [15,154–156], kidneys [16,157–159] and skeletal muscle. Future work is needed to determine the role of MRE in the evaluation of malignant tumors in these organs.

4.6. Therapy response

Recent evidence suggests that MRE may be sensitive to early changes in tumor mechanical properties following treatment. Juge et al. demonstrated that, compared with DWI, MRE is more sensitive to decreased microvessel density (MVD) due to antivascular treatment in a murine model of colon cancer [65]. Microvessel density is a biomarker of tumor aggressiveness and prognosis in colon cancer [160] but no noninvasive technique exists that is directly correlated to MVD during both tumor growth and following therapy. DCE-MRI is related to the perfusion and permeability of blood vessels but not MVD since tumor vessels may be nonfunctional [161]. DWI is used to assess tumor architecture such as cellularity and necrosis. MRE may provide complementary information to existing techniques. This study assessed the ability of MRE to detect changes in tumor viscoelastic properties following antivascular treatment to decrease MVD. The complex shear modulus ($|G^*|$) and apparent diffusion coefficient (ADC) were monitored during tumor growth and following administration of an antivascular agent. During tumor growth, $|G^*|$ increased and was correlated to an increase in MVD while ADC decreased in accordance with increased cellularity. The transition from early to late angiogenic stages could be distinguished by MRE but not by DWI. Within 24 h of administration of an antivascular agent, there was a decrease in $|G^*|$ but no change in ADC, suggesting that MRE may be more sensitive than DWI to early changes in tumor architecture following treatment.

Pepin et al. observed a decrease in tumor shear stiffness within 3 days of chemotherapy treatment in a murine model of non-Hodgkin's lymphoma [162]. A decrease in tumor stiffness was quantified using MRE before a measurable change in volume, providing further evidence that MRE may be more sensitive than existing techniques to early changes in tissue architecture due to tumor response to therapy. In a similar preclinical study, Li et al. demonstrated that MRE may be a biomarker for treatment-induced necrosis [163]. Tumor viscoelastic properties were monitored before and 24 h after administration of a vascular disrupting agent in a human colorectal xenograft. Tumor viscoelasticity decreased significantly within 24 h of treatment while there was no change in tumor ADC, suggesting MRE may be more sensitive than DWI to early tumor response to therapy.

Early assessment of tumor response to therapy is critical in the effective treatment of cancer. The current clinical metric of response is defined by a reduction in tumor volume measured using a single linear summation (Response Evaluation Criteria in Solid Tumors; RECIST) or the bilinear volumetric approach

(WHO) [164]. With the development of more targeted therapies such as signal transduction inhibitors, anatomic imaging and volumetric measurements may not necessarily be the most sensitive measure of response. For example, ^{18}F-fluoro-3-deoxythymidine (^{18}F-FDG) PET to measure tumor metabolic activity has replaced anatomical-based imaging as the standard of care in evaluating gastrointestinal stromal tumor response to imatinib [165]. The results of these preclinical studies demonstrate that MRE provides complementary information to existing imaging techniques and may be useful as a biomarker of response to therapy.

5. Conclusions

Numerous investigations have identified existing and emerging applications for MRE in oncology. MRE is emerging as a noninvasive technique to improve the detection and characterization of malignant tissue due to the different viscoelastic properties between normal and diseased tissue. Alterations in the mechanical properties of cancerous tissue provide a unique contrast mechanism that is quantified using MRE. This contrast provides significant diagnostic potential which has been shown to improve the sensitivity and specificity conventional MR imaging when differentiating malignant from benign tumors in the breast and liver.

It is important to recognize that the viscoelastic properties measured with MRE are directly related to the underlying tissue architecture. This architecture is influenced by multiple factors including extracellular matrix composition, vascular structure and function, cellular density, and interstitial fluid pressure, each of which is altered during malignant transformation. MRE is sensitive to changes in the mechanical properties of tissue and therefore holds great potential for the characterization of malignant neoplasms and for the evaluation of novel therapies. For example, high interstitial pressure is a barrier in the delivery of chemotherapeutic drugs and has been shown to be a predictor of patient outcome [62]. Increased ECM stiffness has been shown to promote the progression of cancer. MRE may be sensitive to these alterations and may provide a source of mechanical contrast for understanding the role of these properties in the progression of malignancy.

Potential clinical applications are continually emerging, including the evaluation of treatment response, monitoring of disease progression, and improved diagnosis of disease. Ongoing work will further refine and optimize MRE for applications in oncology. Application of true three-dimensional imaging and inversion algorithms can improve ability to diagnose focal disease by increasing MRE spatial resolution. Extensive work is being done to develop more sophisticated models of in vivo viscoelastic properties, which may lead to the quantification of additional parameters that characterize tissue properties such as attenuation, anisotropy, and nonlinearity. In summary, emerging evidence indicates that MRE offers valuable quantitative information on the mechanical properties of tissue, and this technique may be especially relevant in the detection and characterization of cancer.

Acknowledgements

We acknowledge Jun Chen and Arvin Arani (Mayo Clinic) and Rajiv Chopra (UT Southwestern Medical Center) for providing Figs. 2 and 5. Funding support for this work was provided by the National Institute of Health Grant EB001981, the Mayo Clinic Center for Individualized Medicine, and the Mayo Graduate School.

References

[1] A.P. Sarvazyan, A.R. Skovoroda, S.Y. Emelianov, J.B. Fowlkes, J.G. Pipe, R.S. Adler, R.B. Buxton, P.L. Carson, Biophysical bases of elasticity imaging, in: J.P. Jones (Ed.), Acoustical Imaging, Plenum Press, New York, 1995, pp. 223–240.
[2] M.B. Barton, R. Harris, S.W. Fletcher, The rational clinical examination. Does this patient have breast cancer? The screening clinical breast examination: should it be done? How?, JAMA 282 (1999) 1270–1280
[3] R. Muthupillai, D.J. Lomas, P.J. Rossman, J.F. Greenleaf, A. Manduca, R.L. Ehman, Magnetic resonance elastography by direct visualization of propagating acoustic strain waves, Science 269 (1995) 1854–1857.
[4] A.R. Padhani, G. Liu, D.M. Koh, T.L. Chenevert, H.C. Thoeny, T. Takahara, A. Dzik-Jurasz, B.D. Ross, M. Van Cauteren, D. Collins, D.A. Hammoud, G.J. Rustin, B. Taouli, P.L. Choyke, Diffusion-weighted magnetic resonance imaging as a cancer biomarker: consensus and recommendations, Neoplasia 11 (2009) 102–125.
[5] L.M. Johnson, B. Turkbey, W.D. Figg, P.L. Choyke, Multiparametric MRI in prostate cancer management, Nat. Rev. Clin. Oncol. 11 (2014) 346–353.
[6] C.L. Sawyers, L.J. van't Veer, Reliable and effective diagnostics are keys to accelerating personalized cancer medicine and transforming cancer care: a policy statement from the american association for cancer research, Clin. Cancer Res. 20 (2014) 4978–4981.
[7] M. Yin, J.A. Talwalkar, K.J. Glaser, A. Manduca, R.C. Grimm, P.J. Rossman, J.L. Fidler, R.L. Ehman, Assessment of hepatic fibrosis with magnetic resonance elastography, Clin. Gastroenterol. Hepatol. 5 (2007) 1207–1213.
[8] L. Huwart, F. Peeters, R. Sinkus, L. Annet, N. Salameh, L.C. ter Beek, Y. Horsmans, B.E. Van Beers, Liver fibrosis: non-invasive assessment with MR elastography, NMR Biomed. 19 (2006) 173–179.
[9] M.C. Murphy, J. Huston, C.R. Jack, K.J. Glaser, M.L. Senjem, J. Chen, A. Manduca, J.P. Felmlee, R.L. Ehman, Measuring the characteristic topography of brain stiffness with magnetic resonance elastography, PLoS ONE 8 (2013) e81668.
[10] I. Sack, B. Beierbach, U. Hamhaber, D. Klatt, J. Braun, Non-invasive measurement of brain viscoelasticity using magnetic resonance elastography, NMR Biomed. 21 (2008) 265–271.
[11] R. Sinkus, J. Lorenzen, D. Schrader, M. Lorenzen, M. Dargatz, D. Holz, High-resolution tensor MR elastography for breast tumour detection, Phys. Med. Biol. 45 (2000) 1649–1664.
[12] A. Kolipaka, K.P. McGee, P.A. Araoz, K.J. Glaser, A. Manduca, A.J. Romano, R.L. Ehman, MR elastography as a method for the assessment of myocardial stiffness: comparison with an established pressure-volume model in a left ventricular model of the heart, Magn. Reson. Med. 62 (2009) 135–140.
[13] I. Sack, J. Rump, T. Elgeti, A. Samani, J. Braun, MR elastography of the human heart: noninvasive assessment of myocardial elasticity changes by shear wave amplitude variations, Magn. Reson. Med. 61 (2009) 668–677.
[14] Y.K. Mariappan, K.J. Glaser, R.D. Hubmayr, A. Manduca, R.L. Ehman, K.P. McGee, MR elastography of human lung parenchyma: technical development, theoretical modeling and in vivo validation, J. Magn. Reson. Imaging 33 (2011) 1351–1361.
[15] J.A. Talwalkar, M. Yin, S.K. Venkatesh, P.J. Rossman, R.C. Grimm, A. Manduca, A.J. Romano, P.S. Kamath, R.L. Ehman, Feasibility of in vivo MR elastographic splenic stiffness measurements in the assessment of portal hypertension, AJR 193 (2009) 122–127.
[16] S.F. Bensamoun, L. Robert, G.E. Leclerc, L. Debernard, F. Charleux, Stiffness imaging of the kidney and adjacent abdominal tissues measured simultaneously using magnetic resonance elastography, Clin. Imaging 35 (2011) 284–287.
[17] Y. Shi, K.J. Glaser, S.K. Venkatesh, E.I. Ben-Abraham, R.L. Ehman, Feasibility of using 3D MR elastography to determine pancreatic stiffness in healthy volunteers, J. Magn. Reson. Imaging (2014).
[18] L. Debernard, J.Y. Hogrel, S.F. Bensamoun, Non-invasive assessment of muscle stiffness with magnetic resonance elastography, Neuromuscul. Disord. 19 (2009) 629–630.
[19] M.M. Bahn, M.D. Brennan, R.S. Bahn, D.S. Dean, J.L. Kugel, R.L. Ehman, Development and application of magnetic resonance elastography of the normal and pathological thyroid gland in vivo, J. Magn. Reson. Imaging 30 (2009) 1151–1154.
[20] S. Venkatesh, R.L. Ehman, Magnetic Resonance Elastography, Springer, New York, New York, RL, 2014.
[21] J. Ophir, I. Cespedes, H. Ponnekanti, Y. Yazdi, X. Li, Elastography: a quantitative method for imaging the elasticity of biological tissues, Ultrason. Imaging 13 (1991) 111–134.
[22] D.E. Jaalouk, J. Lammerding, Mechanotransduction gone awry, Nat. Rev. Mol. Cell Biol. 10 (2009) 63–73.
[23] H. Yu, J.K. Mouw, V.M. Weaver, Forcing form and function: biomechanical regulation of tumor evolution, Trends Cell Biol. 21 (2011) 47–56.
[24] A. Sarvazyan, T.J. Hall, M.W. Urban, M. Fatemi, S.R. Aglyamov, B.S. Garra, An overview of elastography – an emerging branch of medical imaging, Curr. Med. Imaging Rev. 7 (2011) 255–282.
[25] Y.C. Feng, Biomechanics: Mechanical Properties of Living Tissue, Springer, New York, 1993.
[26] Y.K. Mariappan, K.J. Glaser, R.L. Ehman, Magnetic resonance elastography: a review, Clin. Anat. 23 (2010) 497–511.
[27] Z.T.H. Tse, H. Janssen, A. Hamed, M. Ristic, I. Young, M. Lamperth, Magnetic resonance elastography hardware design: a survey, Proc. Inst. Mech. Eng. Part H 223 (2009) 497–514.
[28] E.C. Ehman, P.J. Rossman, S.A. Kruse, A.V. Sahakian, K.J. Glaser, Vibration safety limits for magnetic resonance elastography, Phys. Med. Biol. 53 (2008) 925–935.
[29] J. Bishop, G. Poole, M. Leitch, D.B. Plewes, Magnetic resonance imaging of shear wave propagation in excised tissue, J. Magn. Reson. Imaging 8 (1998) 1257–1265.

[30] K.J. Glaser, A. Manduca, R.L. Ehman, Review of MR elastography applications and recent development, J. Magn. Reson. Imaging 36 (2012) 757–774.
[31] Y.K. Mariappan, K.J. Glaser, A. Manduca, A.J. Romano, S.K. Venkatesh, M. Yin, R.L. Ehman, High-frequency mode conversion technique for stiff lesion detection with magnetic resonance elastography (MRE), Magn. Reson. Med. 62 (2009) 1457–1465.
[32] A. Manduca, T.E. Oliphant, M.A. Dresner, J.L. Mahowald, S.A. Kruse, E. Amromin, J.P. Felmlee, J.F. Greenleaf, R.L. Ehman, Magnetic resonance elastography: non-invasive mapping of tissue elasticity, Med. Image Anal. 5 (2001) 237–254.
[33] R. Muthupillai, R.L. Ehman, Magnetic resonance elastography, Nat. Med. 2 (1996) 601–603.
[34] K.G. Glaser, Ehman R.L., Perspectives on the Development of Elastography, in: S. Venkatesh, R.L. Ehman (Ed.) Magnetic Resonance Elastography, Springer, New York, 2014, pp. 3–13.
[35] S.D. Serai, M. Yin, H. Wang, R.L. Ehman, D.J. Podberesky, Cross-vendor validation of liver magnetic resonance elastography, Abdom. Imaging (2014).
[36] R. Muthupillai, P.J. Rossman, D.J. Lomas, J.F. Greenleaf, S.J. Riederer, R.L. Ehman, Magnetic resonance imaging of transverse acoustic strain waves, Magn. Reson. Med. 36 (1996) 266–274.
[37] A. Manduca, R. Muthupillai, P.J. Rossman, J.F. Greenleaf, R.L. Ehman, Visualization of tissue elasticity by magnetic resonance elastography, in: K. Hones, R. Kinikis (Eds.), Visualization in Biomedical Computing, Springer, 1996, pp. 63–68.
[38] M. Yin, J. Woollard, X. Wang, V.E. Torres, P.C. Harris, C.J. Ward, K.J. Glaser, A. Manduca, R.L. Ehman, Quantitative assessment of hepatic fibrosis in an animal model with magnetic resonance elastography, Magn. Reson. Med. 58 (2007) 346–353.
[39] T.E. Oliphant, A. Manduca, R.L. Ehman, J.F. Greenleaf, Complex-valued stiffness reconstruction for magnetic resonance elastography by algebraic inversion of the differential equation, Magn. Reson. Med. 45 (2001) 299–310.
[40] A. Baghani, S. Salcudean, M. Honarvar, R. Sahebjavaher, R. Rohling, R. Sinkus, Travelling wave expansion: a model fitting approach to the inverse problem of elasticity reconstruction, IEEE Trans. Med. Imaging 30 (2011) 1555–1565.
[41] A. Romano, M. Scheel, S. Hirsch, J. Braun, I. Sack, In vivo waveguide elastography of white matter tracts in the human brain, Magn. Reson. Med. 68 (2012) 1410–1422.
[42] M.M. Doyley, Model-based elastography: a survey of approaches to the inverse elasticity problem, Phys. Med. Biol. 57 (2012) R35–R73.
[43] A.J. Romano, J.A. Bucaro, R.L. Ehman, J.J. Shirron, Evaluation of a material parameter extraction algorithm using MRI-based displacement measurements, IEEE Transact. Ultrason., Ferroel., Freq. Contr. 47 (2000) 1575–1581.
[44] I.M. Perreard, A.J. Pattison, M. Doyley, M.D.J. McGarry, Z. Barani, E.E.W. Van Houten, J.B. Weaver, K.D. Paulsen, Effects of frequency- and direction-dependent elastic materials on linearly elastic MRE image reconstructions, Phys. Med. Biol. 55 (2010) 6801–6815.
[45] E.E.W. Van Houten, M.I. Miga, J.B. Weaver, F.E. Kennedy, K.D. Paulsen, Three-dimensional subzoned-based reconstruction algorithm for MR elastography, Magn. Reson. Med. 45 (2001) 827–837.
[46] M.D.J. McGarry, E.E.W. Van Houten, C.L. Johnson, J.G. Georgiadis, B.P. Sutton, J.B. Weaver, K.D. Paulsen, Multiresolution MR elastography using nonlinear inversion, Med. Phys. 39 (2012) 6388–6396.
[47] P.R. Perrinez, F.E. Kennedy, E.E.W. Van Houten, J.B. Weaver, K.D. Paulsen, Magnetic resonance poroelastography: an algorithm for estimating the mechanical properties of fluid-saturated soft tissues, IEEE Trans. Med. Imaging 29 (2010) 746–755.
[48] D.H. Lee, J.M. Lee, J.K. Han, B.I. Choi, MR elastography of healthy liver parenchyma: normal value and reliability of the liver stiffness value measurement, J. Magn. Reson. Imaging 38 (2013) 1215–1223.
[49] S.K. Venkatesh, M. Yin, R.L. Ehman, Magnetic resonance elastography of liver: technique, analysis, and clinical applications, J. Magn. Reson. Imaging 37 (2013) 544–555.
[50] C.D.G. Hines, T.A. Bley, M.J. Lindstrom, S.B. Reeder, Repeatability of magnetic resonance elastography for quantification of hepatic stiffness, J. Magn. Reson. Imaging 31 (2010) 725–731.
[51] C.D.G. Hines, M.J. Lindstrom, A.K. Varma, S.B. Reeder, Effects of postprandial state and mesenteric blood flow on the repeatability of MR elastography in asymptomatic subjects, J. Magn. Reson. Imaging 33 (2011) 239–244.
[52] N.J. Shire, M. Yin, J. Chen, R.A. Railkar, S. Fox-Bosetti, S.M. Johnson, C.R. Beals, B.J. Dardzinski, S.O. Sanderson, J.A. Talwalkar, R.L. Ehman, Test-retest repeatability of MR elastography for noninvasive liver fibrosis assessment in Hepatitis C, J. Magn. Reson. Imaging 34 (2011) 947–955.
[53] M.C. Murphy, K.J. Glaser, B.D. Bolster, D.V. Litwiller, S.A. Kruse, R.L. Ehman, Cross-Platform Comparison of Brain MRE, in: 19th Annual Meeting of ISMRM, Montreal, 2011.
[54] R.A. Weinberg, The Biology of Cancer, Garland Science, Taylor & Francis Group, New York, NY, 2007.
[55] S. Suresh, Biomechanics and biophysics of cancer cells, Acta Biomater. 3 (2007) 413–438.
[56] M. Lekka, K. Pogoda, J. Gostek, O. Klymenko, S. Prauzner-Bechcicki, J. Wiltowska-Zuber, J. Jaczewska, J. Lekki, Z. Stachura, Cancer cell recognition–mechanical phenotype, Micron 43 (2012) 1259–1266.
[57] Q.S. Li, G.Y. Lee, C.N. Ong, C.T. Lim, AFM indentation study of breast cancer cells, Biochem. Biophys. Res. Commun. 374 (2008) 609–613.
[58] R.K. Jain, Barriers to drug delivery in solid tumors, Sci. Am. 271 (1994) 58–65.
[59] J.S. Byun, K. Gardner, Wounds that will not heal: pervasive cellular reprogramming in cancer, Am. J. Pathol. 182 (2013) 1055–1064.
[60] H.F. Dvorak, Tumors: wounds that do not heal. Similarities between tumor stroma generation and wound healing, New Engl. J. Med. 315 (1986) 1650–1659.
[61] P. Lu, V.M. Weaver, Z. Werb, The extracellular matrix: a dynamic niche in cancer progression, J. Cell Biol. 196 (2012) 395–406.
[62] C.H. Heldin, K. Rubin, K. Pietras, A. Ostman, High interstitial fluid pressure – an obstacle in cancer therapy, Nat. Rev. Cancer 4 (2004) 806–813.
[63] R.K. Jain, Delivery of molecular and cellular medicine to solid tumors, Adv. Drug Deliv. Rev. 46 (2001) 149–168.
[64] R.K. Jain, Normalizing tumor vasculature with anti-angiogenic therapy: a new paradigm for combination therapy, Nat. Med. 7 (2001) 987–989.
[65] L. Juge, B.T. Doan, J. Seguin, M. Albuquerque, B. Larrat, N. Mignet, G.G. Chabot, D. Scherman, V. Paradis, V. Vilgrain, B.E. Van Beers, R. Sinkus, Colon tumor growth and antivascular treatment in mice: complementary assessment with MR elastography and diffusion-weighted MR imaging, Radiology 264 (2012) 436–444.
[66] J.M. Llovet, A. Burroughs, J. Bruix, Hepatocellular carcinoma, Lancet 362 (2003) 1907–1917.
[67] J. Bruix, M. Sherman, J.M. Llovet, M. Beaugrand, R. Lencioni, A.K. Burroughs, E. Christensen, L. Pagliaro, M. Colombo, J. Rodes, Clinical management of hepatocellular carcinoma. Conclusions of the Barcelona-2000 EASL conference. European association for the study of the liver, J. Hepatol. 35 (2001) 421–430.
[68] K. Hoyt, B. Castaneda, M. Zhang, P. Nigwekar, P.A. di Sant'agnese, J.V. Joseph, J. Strang, D.J. Rubens, K.J. Parker, Tissue elasticity properties as biomarkers for prostate cancer, Cancer Biomark 4 (2008) 213–225.
[69] J.A. Tuxhorn, G.E. Ayala, D.R. Rowley, Reactive stroma in prostate cancer progression, J. Urol. 166 (2001) 2472–2483.
[70] J.A. Tuxhorn, G.E. Ayala, M.J. Smith, V.C. Smith, T.D. Dang, D.R. Rowley, Reactive stroma in human prostate cancer: induction of myofibroblast phenotype and extracellular matrix remodeling, Clin. Cancer Res. 8 (2002) 2912–2923.
[71] N. Burns-Cox, N.C. Avery, J.C. Gingell, A.J. Bailey, Changes in collagen metabolism in prostate cancer: a host response that may alter progression, J. Urol. 166 (2001) 1698–1701.
[72] J. Zhang, J. Liu, Tumor stroma as targets for cancer therapy, Pharmacol. Ther. 137 (2013) 200–215.
[73] S. Ferretti, P.R. Allegrini, M.M. Becquet, P.M. McSheehy, Tumor interstitial fluid pressure as an early-response marker for anticancer therapeutics, Neoplasia 11 (2009) 874–881.
[74] T.A. Krouskop, T.M. Wheeler, F. Kallel, B.S. Garra, T. Hall, Elastic moduli of breast and prostate tissues under compression, Ultrason. Imaging 20 (1998) 260–274.
[75] A. Samani, J. Zubovits, D.B. Plewes, Elastic moduli of normal and pathological human breast tissues: an inversion-technique-based investigation of 169 samples, Phys. Med. Biol. 52 (2007) 1565–1576.
[76] E. Warner, Clinical practice. Breast-cancer screening, New Engl. J. Med. 365 (2011) 1025–1032.
[77] J.S. Drukteinis, B.P. Mooney, C.I. Flowers, R.A. Gatenby, Beyond mammography: new frontiers in breast cancer screening, Am. J. Med. 126 (2013) 472–479.
[78] E.J. Granader, B. Dwamena, R.C. Carlos, MRI and mammography surveillance of women at increased risk for breast cancer: recommendations using an evidence-based approach, Acad. Radiol. 15 (2008) 1590–1595.
[79] C. Kuhl, The current status of breast MR imaging. Part I. Choice of technique, image interpretation, diagnostic accuracy, and transfer to clinical practice, Radiology 244 (2007) 356–378.
[80] O. Alagoz, J. Chhatwal, E.S. Burnside, Optimal policies for reducing unnecessary follow-up mammography exams in breast cancer diagnosis, Decis. Anal. 10 (2013) 200–224.
[81] K.C. Siegmann, B. Kramer, C. Claussen, Current status and new developments in breast MRI, Breast Care (Basel) 6 (2011) 87–92.
[82] R.J. Hooley, L.M. Scoutt, L.E. Philpotts, Breast ultrasonography: state of the art, Radiology 268 (2013) 642–659.
[83] B.S. Garra, E.I. Cespedes, J. Ophir, S.R. Spratt, R.A. Zuurbier, C.M. Magnant, M.F. Pennanen, Elastography of breast lesions: initial clinical results, Radiology 202 (1997) 79–86.
[84] A. Evans, P. Whelehan, K. Thomson, K. Brauer, L. Jordan, C. Purdie, D. McLean, L. Baker, S. Vinnicombe, A. Thompson, Differentiating benign from malignant solid breast masses: value of shear wave elastography according to lesion stiffness combined with greyscale ultrasound according to BI-RADS classification, Br. J. Cancer 107 (2012) 224–229.
[85] G. Sadigh, R.C. Carlos, C.H. Neal, B.A. Dwamena, Accuracy of quantitative ultrasound elastography for differentiation of malignant and benign breast abnormalities: a meta-analysis, Breast Cancer Res. Treat. 134 (2012) 923–931.
[86] R.G. Barr, S. Destounis, L.B. Lackey 2nd, W.E. Svensson, C. Balleyguier, C. Smith, Evaluation of breast lesions using sonographic elasticity imaging: a multicenter trial, J. Ultrasound Med. 31 (2012) 281–287.
[87] T. Uematsu, Ultrasonographic findings of missed breast cancer: pitfalls and pearls, Breast Cancer 21 (2014) 10–19.
[88] S.H. Lee, J.M. Chang, N. Cho, H.R. Koo, A. Yi, S.J. Kim, J.H. Youk, E.J. Son, S.H. Choi, S.H. Kook, J. Chung, E.S. Cha, J.S. Park, H.K. Jung, K.H. Ko, H.Y. Choi, E.B. Ryu, W.K. Moon, Practice guideline for the performance of breast ultrasound elastography, Ultrasonography 33 (2014) 3–10.

[89] J.M. Chang, W.K. Moon, N. Cho, S.J. Kim, Breast mass evaluation: factors influencing the quality of US elastography, Radiology 259 (2011) 59–64.
[90] J. Lorenzen, R. Sinkus, M. Biesterfeldt, G. Adam, Menstrual-cycle dependence of breast parenchyma elasticity: estimation with magnetic resonance elastography of breast tissue during the menstrual cycle, Invest. Radiol. 38 (2003) 236–240.
[91] A.L. McKnight, J.L. Kugel, P.J. Rossman, A. Manduca, L.C. Hartmann, R.L. Ehman, MR elastography of breast cancer: preliminary results, AJR 178 (2002) 1411–1417.
[92] J. Lorenzen, R. Sinkus, M. Lorenzen, M. Dargatz, C. Leussler, P. Roschmann, G. Adam, MR elastography of the breast: preliminary clinical results, Fortschr. Rontgenstr. 174 (2002) 830–834.
[93] R. Sinkus, M. Tanter, S. Catheline, J. Lorenzen, C. Kuhl, E. Sondermann, M. Fink, Imaging anisotropic and viscous properties of breast tissue by magnetic resonance elastography, Magn. Reson. Med. 53 (2005) 372–387.
[94] R. Sinkus, M. Tanter, T. Xydeas, S. Catheline, J. Bercoff, M. Fink, Viscoelastic shear properties of in vivo breast lesions measured by MR elastography, Magn. Reson. Imaging 23 (2005) 159–165.
[95] T. Xydeas, K. Siegmann, R. Sinkus, U. Krainick-Strobel, S. Miller, C.D. Claussen, Magnetic resonance elastography of the breast correlation of signal intensity data with viscoelastic properties, Invest. Radiol. 40 (2005) 412–420.
[96] R. Sinkus, K. Siegmann, T. Xydeas, M. Tanter, C. Claussen, M. Fink, MR elastography of breast lesions: understanding the solid/liquid duality can improve the specificity of contrast-enhanced MR mammography, Magn. Reson. Med. 58 (2007) 1135–1144.
[97] K. Siegmann, T. Xydeas, R. Sinkus, B. Kraemer, U. Vogel, C. Claussen, Diagnostic value of MR elastography in addition to contrast-enhanced MR imaging of the breast -initial clinical results, Eur. Radiol. 20 (2010) 318–325.
[98] American Cancer Society recommendations for early breast cancer detection in women without breast symptoms, in: Breast Cancer Prevention and Early Detection, American Cancer Society, 2014.
[99] S.K. Venkatesh, M. Yin, J.F. Glockner, N. Takahashi, P.A. Araoz, J.A. Talwalkar, R.L. Ehman, MR elastography of liver tumors: preliminary results, AJR 190 (2008) 1534–1540.
[100] L. Huwart, C. Sempoux, E. Vicaut, N. Salameh, L. Annet, E. Danse, F. Peeters, L.C. ter Beek, J. Rahier, R. Sinkus, Y. Horsmans, B.E. Van Beers, Magnetic resonance elastography for the noninvasive staging of liver fibrosis, Gastroenterology 135 (2008) 32–40.
[101] O. Rouviere, M. Yin, M.A. Dresner, P.J. Rossman, L.J. Burgart, J.L. Fidler, R.L. Ehman, MR elastography of the liver: preliminary results, Radiology 240 (2006) 440–448.
[102] D. Elias, L. Sideris, M. Pocard, T. de Baere, C. Dromain, N. Lassau, P. Lasser, Incidence of unsuspected and treatable metastatic disease associated with operable colorectal liver metastases discovered only at laparotomy (and not treated when performing percutaneous radiofrequency ablation), Ann. Surg. Oncol. 12 (2005) 298–302.
[103] S.K. Venkatesh, M. Yin, R.L. Ehman, Magnetic resonance elastography of liver: clinical applications, J. Comput. Assist. Tomogr. 37 (2013) 887–896.
[104] P. Garteiser, S. Doblas, J.L. Daire, M. Wagner, H. Leitao, V. Vilgrain, R. Sinkus, B.E. Van Beers, MR elastography of liver tumours: value of viscoelastic properties for tumour characterisation, Eur. Radiol. 22 (2012) 2169–2177.
[105] J. Bruix, M. Sherman, Management of hepatocellular carcinoma, Hepatology 42 (2005) 1208–1236.
[106] J.A. Talwalkar, P.S. Kamath, Influence of recent advances in medical management on clinical outcomes of cirrhosis, Mayo Clin. Proc. 80 (2005) 1501–1508.
[107] R. Masuzaki, R. Tateishi, H. Yoshida, S. Sato, N. Kato, F. Kanai, Y. Sugioka, H. Ikeda, S. Shiina, T. Kawabe, M. Omata, Risk assessment of hepatocellular carcinoma in chronic hepatitis C patients by transient elastography, J. Clin. Gastroenterol. 42 (2008) 839–843.
[108] U. Motosugi, T. Ichikawa, T. Koshiishi, K. Sano, H. Morisaka, S. Ichikawa, N. Enomoto, M. Matsuda, H. Fujii, T. Araki, Liver stiffness measured by magnetic resonance elastography as a risk factor for hepatocellular carcinoma: a preliminary case-control study, Eur. Radiol. 23 (2013) 156–162.
[109] J. Wuerfel, F. Paul, B. Beierbach, U. Hamhaber, D. Klatt, S. Papazoglou, F. Zipp, P. Martus, J. Braun, I. Sack, MR-elastography reveals degradation of tissue integrity in multiple sclerosis, NeuroImage 49 (2010) 2520–2525.
[110] E.H. Clayton, J.R. Garbow, P.V. Bayly, Frequency-dependent viscoelastic parameters of mouse brain tissue estimated by MR elastography, Phys. Med. Biol. 56 (2011) 2391–2406.
[111] Y. Feng, E.H. Clayton, Y. Chang, R.J. Okamoto, P.V. Bayly, Viscoelastic properties of the ferret brain measured in vivo at multiple frequencies by magnetic resonance elastography, J. Biomech. 46 (2013) 863–870.
[112] K. Riek, J.M. Millward, I. Hamann, S. Mueller, C.F. Pfueller, F. Paul, J. Braun, C. Infante-Duarte, I. Sack, Magnetic resonance elastography reveals altered brain viscoelasticity in experimental autoimmune encephalomyelitis, NeuroImage: Clin. 1 (2012) 81–90.
[113] T. Kaster, I. Sack, A. Samani, Measurement of the hyperelastic properties of ex vivo brain tissue slices, J. Biomech. 44 (2011) 1158–1163.
[114] S.A. Kruse, G.H. Rose, K.J. Glaser, A. Manduca, J.P. Felmlee, C.R. Jack, R.L. Ehman, Magnetic resonance elastography of the brain, NeuroImage 39 (2008) 231–237.
[115] M.A. Green, L.E. Bilston, R. Sinkus, *In vivo* brain viscoelastic properties measured by magnetic resonance elastography, NMR Biomed. 21 (2008) 755–764.
[116] I. Sack, B. Beierbach, J. Wuerfel, D. Klatt, U. Hamhaber, S. Papazoglou, P. Martus, J. Braun, The impact on aging and gender on brain viscoelasticity, NeuroImage 46 (2009) 652–657.
[117] P. Latta, M.L.H. Gruwel, P. Debergue, B. Matwiy, U.N. Sboto-Frankenstein, B. Tomanek, Convertible pneumatic actuator for magnetic resonance elastography of the brain, Magn. Reson. Imaging 29 (2011) 147–152.
[118] D.K.W. Yeung, K.S. Bhatia, Y.Y.P. Lee, A.D. King, P. Garteiser, R. Sinkus, A.T. Ahuja, MR elastography of the head and neck: driver design and initial results, Magn. Reson. Imaging 31 (2013) 624–629.
[119] L. Xu, Y. Lin, N. Xi, H. Shen, P.Y. Gao, Magnetic resonance elastography of the human brain: a preliminary study, Acta Radiol. 1 (2007) 112–115.
[120] E. Ruoslahti, Brain extracellular matrix, Glycobiology 6 (1996) 489–492.
[121] J. Guo, S. Hirsch, A. Fehlner, S. Papazoglou, M. Scheel, J. Braun, I. Sack, Towards an elastographic atlas of brain anatomy, PLoS ONE 8 (2013) e71807.
[122] S. Hirsch, J. Guo, R. Reiter, S. Papazoglou, T. Kroencke, J. Braun, I. Sack, MR elastography of the liver and the spleen using a piezoelectric driver, single-shot wave-field acquisition, and multifrequency dual parameter reconstruction, Magn. Reson. Med. 71 (2014) 267–277.
[123] M.C. Murphy, J. Huston, K.J. Glaser, A. Manduca, F.B. Meyer, G. Lanzino, J.M. Morris, J.P. Felmlee, R.L. Ehman, Preoperative assessment of meningioma stiffness using magnetic resonance elastography, J. Neuro. 118 (2013) 643–648.
[124] L. Xu, Y. Lin, J.C. Han, Z.N. Xi, H. Shen, P.Y. Gao, Magnetic resonance elastography of brain tumors: preliminary results, Acta Radiol. 37 (2007) 327–330.
[125] J.N. Scott, P.M. Brasher, R.J. Sevick, N.B. Rewcastle, P.A. Forsyth, How often are nonenhancing supratentorial gliomas malignant? A population study, Neurology 59 (2002) 947–949.
[126] M. Reiss-Zimmermann, K.J. Streitberger, I. Sack, J. Braun, F. Arlt, D. Fritzsch, K.T. Hoffmann, High Resolution Imaging of Viscoelastic Properties of Intracranial Tumours by Multi-Frequency Magnetic Resonance Elastography, Clin Neuroradiol, (2014).
[127] J. Huston III, Magnetic resonance elastography of the brain, in: S.K. Venkatesh, R.L. Ehman (Eds.), Magnetic Resonance Elastography, Springer Science, New York, 2014, pp. 89–98.
[128] A.R. Padhani, C.M. Nutting, Why do we need more accurate intraprostatic localization of cancer?, Br J. Radiol. 76 (2003) 585–586.
[129] J.R. Thornbury, D.K. Ornstein, P.L. Choyke, C.P. Langlotz, J.C. Weinreb, Prostate cancer: what is the future role for imaging?, AJR Am J. Roentgenol. 176 (2001) 17–22.
[130] T.J. Wilt, R. MacDonald, I. Rutks, T.A. Shamliyan, B.C. Taylor, R.L. Kane, Systematic review: comparative effectiveness and harms of treatments for clinically localized prostate cancer, Ann. Intern. Med. 148 (2008) 435–448.
[131] J.V. Hegde, R.V. Mulkern, L.P. Panych, F.M. Fennessy, A. Fedorov, S.E. Maier, C.M. Tempany, Multiparametric MRI of prostate cancer: an update on state-of-the-art techniques and their performance in detecting and localizing prostate cancer, J. Magn. Reson. Imaging 37 (2013) 1035–1054.
[132] M. Zhang, P. Nigwekar, B. Castaneda, K. Hoyt, J.V. Joseph, A. di Sant'Agnese, E.M. Messing, J.G. Strang, D.J. Rubens, K.J. Parker, Quantitative characterization of viscoelastic properties of human prostate correlated with histology, Ultrasound Med. Biol. 34 (2008) 1033–1042.
[133] J. Kemper, R. Sinkus, J. Lorenzen, C. Nolte-Ernsting, A. Stork, G. Adam, MR elastography of the prostate: initial in vivo application, RoFo; Fortschritte auf dem Gebiete der Rontgenstrahlen und der Nuklearmedizin 176 (2004) 1094–1099.
[134] R. Chopra, A. Arani, Y. Huang, M. Musquera, J. Wachsmuth, M. Bronskill, D.B. Plewes, In vivo MR elastography of the prostate gland using a transurethal actuator, Magn. Reson. Med. 62 (2009) 665–671.
[135] A. Arani, D. Plewes, R. Chopra, Transurethral prostate magnetic resonance elastography: prospective imaging requirements, Magn. Reson. Med. 65 (2011) 340–349.
[136] T.A. Stamey, F.S. Freiha, J.E. McNeal, E.A. Redwine, A.S. Whittemore, H.P. Schmid, Localized prostate cancer. Relationship of tumor volume to clinical significance for treatment of prostate cancer, Cancer 71 (1993) 933–938.
[137] A.M. Wise, T.A. Stamey, J.E. McNeal, J.L. Clayton, Morphologic and clinical significance of multifocal prostate cancers in radical prostatectomy specimens, Urology 60 (2002) 264–269.
[138] A. Arani, D. Plewes, A. Krieger, R. Chopra, The feasibility of endorectal MR elastography for prostate cancer localization, Magn. Reson. Med. 66 (2011) 1649–1657.
[139] A. Arani, M. Da Rosa, E. Ramsay, D.B. Plewes, M.A. Haider, R. Chopra, Incorporating endorectal MR elastography into multi-parametric MRI for prostate cancer imaging: initial feasibility in volunteers, J. Magn. Reson. Imaging 38 (2013) 1251–1260.
[140] R.S. Sahebjavaher, A. Baghani, M. Honarvar, R. Sinkus, S.E. Salcudean, Transperineal prostate MR elastography: initial in vivo results, Magn. Reson. Med. 69 (2013) 411–420.
[141] S. Li, M. Chen, W. Wang, W. Zhao, J. Wang, X. Zhao, C. Zhou, A feasibility study of MR elastography in the diagnosis of prostate cancer at 3.0T, Acta Radiol. 52 (2011) 354–358.
[142] R.S. Sahebjavaher, G. Nir, M. Honarvar, L.O. Gagnon, J. Ischia, E.C. Jones, S.D. Chang, L. Fazli, S.L. Goldenberg, R. Rohling, P. Kozlowski, R. Sinkus, S.E. Salcudean, MR elastography of prostate cancer: quantitative comparison with histopathology and repeatability of methods, NMR Biomed. 28 (2015) 124–139.

[143] M. Ghajarzadeh, F. Sodagari, M. Shakiba, Diagnostic accuracy of sonoelastography in detecting malignant thyroid nodules: a systematic review and meta-analysis, AJR Am. J. Roentgenol. 202 (2014) W379–W389.
[144] V. Cantisani, P. Lodise, H. Grazhdani, E. Mancuso, E. Maggini, G. Di Rocco, F. D'Ambrosio, F. Calliada, A. Redler, P. Ricci, C. Catalano, Ultrasound elastography in the evaluation of thyroid pathology. Current status, Eur. J. Radiol. 83 (2014) 420–428.
[145] P.V. Lippolis, S. Tognini, G. Materazzi, A. Polini, R. Mancini, C.E. Ambrosini, A. Dardano, F. Basolo, M. Seccia, P. Miccoli, F. Monzani, Is elastography actually useful in the presurgical selection of thyroid nodules with indeterminate cytology?, J Clin. Endocrinol. Metab. 96 (2011) E1826–E1830.
[146] E.A. Stewart, F.A. Taran, J. Chen, B.S. Gostout, D.A. Woodrum, J.P. Felmlee, R.L. Ehman, Magnetic resonance elastography of uterine leiomyomas: a feasibility study, Fertil. Steril. 95 (2011) 281–284.
[147] C.L. Walker, E.A. Stewart, Uterine fibroids: the elephant in the room, Science 308 (2005) 1589–1592.
[148] N.C. Institute, SEER Stat Fact Sheets: Pancreas Cancer, in: Cancer Statsistics, 2014.
[149] P. Tummala, O. Junaidi, B. Agarwal, Imaging of pancreatic cancer: an overview, J. Gastrointest Oncol. 2 (2011) 168–174.
[150] J. Chen, D.A. Woodrum, K.J. Glaser, M.C. Murphy, K. Gorny, R.L. Ehman, Assessment of in vivo laser ablation using MR elastography with an inertial driver, Magn. Reson. Med. 72 (2014) 59–67.
[151] T. Wu, J.P. Felmlee, J.F. Greenleaf, S.J. Riederer, R.L. Ehman, Assessment of thermal tissue ablation with MR elastography, Magn. Reson. Med. 45 (2001) 80–87.
[152] Y. Le, K.J. Glaser, O. Rouviere, R.L. Ehman, J.P. Felmlee, Feasibility of simultaneous temperature and tissue stiffness detection by MRE, Magn. Reson. Med. 55 (2006) 700–705.
[153] Y. Le, K.J. Glaser, O. Rouviere, K.R. Gorny, S. Chen, A. Manduca, R.L. Ehman, J.P. Felmlee, Preliminary assessment of one-dimensional MR elastography for use in monitoring focused ultrasound therapy, Phys. Med. Biol. 52 (2007) 5909–5919.
[154] L. Mannelli, E. Godfrey, I. Joubert, A.J. Patterson, M.J. Graves, F.A. Gallagher, D.J. Lomas, MR elastography: spleen stiffness measurements in healthy volunteers-preliminary experience, AJR 195 (2010) 387–392.
[155] G.I. Nedredal, M. Yin, T. McKenzie, J. Lillegard, J. Luebke-Wheeler, J.A. Talwalkar, R.L. Ehman, S.L. Nyberg, Portal hypertension correlates with splenic stiffness as measured with MR elastography, J. Magn. Reson. Imaging 34 (2011) 79–87.
[156] H. Morisaka, U. Motosugi, S. Ichikawa, K. Sano, T. Ichikawa, N. Enomoto, Association of splenic MR elastographic findings with gastroesophageal varices in patients with chronic liver disease, J. Magn. Reson. Imaging 41 (2015) 117–124.
[157] O. Rouviere, R. Souchon, G. Pagnoux, J.-M. Menager, J.Y. Chapelon, Magnetic resonance elastography of the kidneys: feasibility and reproducibility in young healthy adults, J. Magn. Reson. Imaging 34 (2011) 880–886.
[158] L. Warner, M. Yin, K.J. Glaser, J.A. Woollard, C.A. Carrascal, M.J. Korsmo, J.A. Crane, R.L. Ehman, L.O. Lerman, Noninvasive in vivo assessment of renal tissue elasticity during graded renal ischemia using MR elastography, Invest. Radiol. 46 (2011) 509–514.
[159] C.U. Lee, J.F. Glockner, K.J. Glaser, M. Yin, J. Chen, A. Kawashima, B. Kim, W.K. Kremers, R.L. Ehman, J.M. Gloor, MR elastography in renal transplant patients and correlation with renal allograft biopsy: a feasibility study, Acad. Radiol. 19 (2012) 834–841.
[160] S.C. Oliveira, K.K. Machado, J. Sabbaga, P.M. Hoff, Integration of anti-vascular endothelial growth factor therapies with cytotoxic chemotherapy in the treatment of colorectal cancer, Cancer J. 16 (2010) 220–225.
[161] O. Feron, Targeting the tumor vascular compartment to improve conventional cancer therapy, Trends Pharmacol. Sci. 25 (2004) 536–542.
[162] K.M. Pepin, J. Chen, K.J. Glaser, Y.K. Mariappan, B. Reuland, S. Ziesmer, R. Carter, S.M. Ansell, R.L. Ehman, K.P. McGee, MR elastography derived shear stiffness - a new imaging biomarker for the assessment of early tumor response to chemotherapy, Magn. Reson. Med. 71 (2014) 1834–1840.
[163] J. Li, Y. Jamin, J.K.R. Boult, C. Cummings, J.C. Waterton, J. Ulloa, R. Sinkus, J.C. Bamber, S.P. Robinson, Tumour biomechanical response to the vascular disrupting agent ZD6126 in vivo assessed by magnetic resonance elastography, Br. J. Cancer 110 (2014) 1727–1732.
[164] C.C. Jaffe, Measures of response: RECIST, WHO, and new alternatives, J. Clin. Oncol. 24 (2006) 3245–3251.
[165] A.D. Van den Abbeele, The lessons of GIST–PET and PET/CT: a new paradigm for imaging, Oncologist 13 (Suppl. 2) (2008) 8–13.

Glossary of abbreviations

3DMMRE: three-dimensional multifrequency magnetic resonance elastography
^{18}F-FDG: ^{18}F-fluro-3-deoxythymidine
ADC: apparent diffusion coefficient
AUC: area under the curve
CE-MRI: contrast-enhanced magnetic resonance imaging
DCE-MRI: dynamic contrast enhanced magnetic resonance imaging
DI: direct inversion
DWI: diffusion weighted imaging
ECM: extracellular matrix
EPI: echo planar imaging
FEM: finite element modeling
GRE: gradient echo
HCC: hepatocellular carcinoma
LFE: local frequency estimation
MDEV: multi-frequency dual elasto-visco
MEG: motion encoding gradient
MPMRI: multi-parametric magnetic resonance imaging
MRI: magnetic resonance imaging
MRE: magnetic resonance elastography
MRSI: magnetic resonance spectroscopic imaging
MVD: microvessel density
PG: phase gradient
ROI: region of interest
RECIST: response evaluation criteria in solid tumors
SE: spin-echo
SNR: signal-to-noise ratio
WHO: world health organization